An ancient divide in outer membrane tethering systems in bacteria suggests a mechanism for the diderm-to-monoderm transition

Jerzy Witwinowski, Anna Sartori-Rupp, Najwa Taib, Nika Pende, To Nam Tham, Daniel Poppleton, Jean-Marc Ghigo, Christophe Beloin, Simonetta Gribaldo

An ancient divide in outer membrane tethering systems in Bacteria suggests a possible mechanism for the diderm-to-monoderm transition

Jerzy WITWINOWSKI[1], Anna SARTORI-RUPP[3,+], Najwa TAIB[1,4,+], Nika PENDE[1], To Nam THAM[1], Daniel POPPLETON[1,5], Jean-Marc GHIGO[2], Christophe BELOIN[2*], Simonetta GRIBALDO[1*]

[1] Institut Pasteur, Université de Paris, UMR CNRS2001, Unit Evolutionary Biology of the Microbial Cell, 75015 Paris, France

[2] Institut Pasteur, Université de Paris, UMR CNRS2001, Genetics of Biofilms Laboratory, 75015 Paris, France

[3] Institut Pasteur, Université de Paris, Unit of Technology and Service Ultra-structural Bio-Imaging, 75015 Paris, France

[4] Institut Pasteur, Université de Paris, Hub Bioinformatics and Biostatistics, F-75015 Paris, France

[5] Sorbonne Université, Collège doctoral, F-75005 Paris, France

*Corresponding authors:

christophe.beloin@pasteur.fr

simonetta.gribaldo@pasteur.fr

[+] These authors contributed equally to this work

Abstract

Recent data support the hypothesis that Gram-positive bacteria (monoderms) arose from Gram-negatives (diderms) through loss of the outer membrane (OM), but how this happened remains unknown. As tethering of the OM is essential for cell envelope stability in diderm bacteria, its destabilization may have been involved in this transition. Here, we present an in-depth analysis of the four known main OM tethering systems across the Tree of Bacteria (ToB). We show that the presence of such systems follows the ToB with a bimodal distribution matching the deepest phylogenetic divergence between Terrabacteria and Gracilicutes. Whereas the lipoprotein Pal is restricted to the Gracilicutes along with a more sporadic occurrence of OmpA, and Braun's lipoprotein Lpp is present only in a subclade of Gammaproteobacteria, diderm Terrabacteria display as the main system the OmpM protein. We propose an evolutionary scenario whereby OmpM represents a simple, ancestral OM tethering system that was later replaced by one based on Pal following the emergence of the Lol machinery to deliver lipoproteins to the OM, with OmpA as a possible transition state. We speculate that the existence of only one main OM tethering system in the Terrabacteria would have allowed the multiple OM losses specifically inferred in this clade through OmpM perturbation, and we provide experimental support for this hypothesis by inactivating all four *ompM* gene copies in the genetically tractable diderm Firmicute *Veillonella parvula*. High-resolution imaging and tomogram reconstructions reveal a non-lethal phenotype in which vast portions of the OM detach from the cells, forming huge vesicles with an inflated periplasm shared by multiple dividing cells. Together, our results highlight an ancient shift of OM tethering systems in bacterial evolution and suggest a possible mechanism for OM loss and the multiple emergences of the monoderm phenotype from diderm ancestors.

Introduction

The shift between monoderms and diderms is one of the major transitions in the evolution of Bacteria (for two recent reviews see [1] and [2]). Growing evidence that the majority of bacterial phyla are diderms, and that monoderms do not constitute a monophyletic clade suggests that the outer membrane (OM) is an ancestral character that was lost multiple times during evolution [1,3,4]. Although the mechanisms are unknown, one of them could have involved destabilization of OM attachment [5].

In diderm bacteria, tethering of the OM to the cell wall is of fundamental importance to preserve cell envelope integrity. OM tethering has been mostly studied in *Escherichia coli*, where at least three different systems are identified (**Figure 1**). The best known is Braun's lipoprotein (Lpp), which forms a covalent link between the OM and peptidoglycan (PG) [6,7]. Lpp mutants present increased sensitivity to membrane stress and higher OM permeability with bleb formation and hypervesiculation in minimal media [8–11]. A second OM tethering system is based on the Pal lipoprotein, which attaches non-covalently both to PG and to the inner membrane protein TolB [10,12,13]. Pal mutants display similar, yet more severe defects than Lpp mutants, including problems with OM constriction at the division plane, also considering that this protein plays multiple cellular functions [10,11,14–16]. Finally, it was demonstrated that the beta barrel OM protein OmpA, sharing a homologous PG-binding domain with Pal, also plays a role in OM attachment in *E. coli* [10,17,18]. In *E. coli* the three systems are at least partially redundant as overexpression of Pal or OmpA suppresses the defects of the *lpp* null mutant[10,13,17,18].

Recent analyses have shown that the most ancient divide in Bacteria likely occurred between two large clades, the Terrabacteria (which encompass both monoderm and diderm phyla, like Cyanobacteria, Firmicutes, Actinobacteria,

Synergistetes, Thermus/Deinococcus, Thermotogae, Chloroflexi, the Candidate Phyla Radiation/CPR) and the Gracilicutes (which include only diderm phyla, such as Proteobacteria, the Planctomycetes/Verrucomicrobia/Chlamydiae superphylum, Bacteroidetes, Spirochaetes) [1,3,4]. Within Terrabacteria, the Firmicutes (low GC Gram-positives) represent an ideal model to study the diderm to monoderm transition: they comprise in fact at least three independent clades that display an OM with lipopolysaccharide: the *Negativicutes*, the *Halanaerobiales* and the *Limnochordia* [1,3,19,20]. We have recently proposed that the OM is an ancestral character of all Firmicutes and was lost repeatedly during their diversification, giving rise to the classical monoderm cell envelope in this phylum [1,3,20]. Diderm Firmicutes lack homologues of Lpp and Pal, but instead possess a fourth type of OM attachment (**Figure 1**). It was first characterized by *in vitro* analysis of a recombinant protein from the Negativicute *Selenomonas ruminantium*, originally named Mep45 (Major Envelope Protein of 45 kDa) and later OmpM [21–24]. OmpM is composed of a beta barrel that inserts into the OM and an N-terminal S-Layer Homology (SLH) domain that binds *in vitro* to PG modified with aliphatic polyamines such as cadaverine or putrescine [23,25,26]. OmpM homologues are present in all diderm Firmicute genomes, frequently in multiple copies and often displaying a conserved genomic context together with other proteins related to OM biogenesis and maintenance [1,3,20]. The first proteomic characterization of the OM in the Negativicute *Veillonella parvula* DSM2008 showed that two of its four OmpM proteins are among the most abundant OM components [27].

Interestingly, OmpM proteins seem to be present in other diderm phyla within the Terrabacteria. In *Synechococcus* (Cyanobacteria), it was shown that proteins composed of a periplasmic SLH domain and an OM beta-barrel (an architecture, which defines OmpM) attach the OM to the PG and their depletion leads to OM stability

defects [28,29]. Similarly, a protein bearing the same architecture, named Slp, was identified in *Thermus thermophilus* (Deinococcus/Thermus), and shown to be involved in the attachment of the outer layer of the cell envelope, although not described at the time as a *bona fide* OM [30,31]. However, cadaverination of PG does not seem to be involved in either of these bacteria, instead the SLH domain of OmpM recognizes pyruvylated secondary cell wall polymers, and deletion of the pyruvyl transferase responsible for this modification (CsaB) led to the same phenotype as deletion/depletion of the OmpM homolog [29,32]. Finally, two proteins, Ompα and Ompβ, were identified as major OM components in the Thermotogae, each corresponding to the SLH and porin domains, respectively, but lack of genetic tools has prevented the construction and analysis of mutants [33].

The existence of four main OM tethering systems in Bacteria poses the question of when they originated and how they evolved. To this aim, we explored their occurrence and evolution across all Bacteria, and we complemented this analysis by experimental inactivation of OmpM in *V. parvula*. Together, our results highlight a major and ancient divide in the way bacteria tether their OM, and allow us to discuss the hypothesis that perturbation of OmpM-based OM tethering was a possible mechanism for the repeated OM losses and transitions to the monoderm phenotype, which occurred specifically in the Terrabacteria. We propose diderm Firmicutes as ideal models to understand the mechanisms involved in OM stability and maintenance, opening the way to replay the monoderm/diderm transition in the laboratory.

Results

OM tethering systems display a bimodal distribution

We carried out an in-depth analysis of the four main OM attachment systems (OmpM, Lpp, Pal, OmpA) across 1093 genomes representing all current bacterial diversity and mapped them onto a reference phylogeny of Bacteria (Supplementary Data Sheet 1A and Figure 2). Strikingly, we could identify OmpM homologues in all diderm Terrabacteria phyla, including diderm Firmicutes (**Figure 2a**, light blue dots), but never in the Gracilicutes.

In agreement with the experimental characterizations mentioned above, we detected OmpM homologues in Deinococcus/Thermus, as well as in Cyanobacteria and their uncultured sister clades (Figure 2a). Cyanobacteria have two paralogues of OmpM, which were differently retained across species (Supplementary Figure S1a and Supplementary Results and Discussion 1.1). We identified Ompα and Ompβ in all Thermotogae and their neighbor candidate phyla Bipolaricaulota and Fraserbacteria (**Figure 2**, darker blue dots), and phylogenetic analysis suggests that they are *bona fide* homologues of canonical OmpM (Supplementary Figure S1 and Supplementary Results and Discussion 1.2). Finally, multiple copies of OmpM are often present in the *Negativicutes* (Extended Data Figure ED1, Supplementary Data Sheet 1C, and Supplementary Results and Discussion 1.3).

In contrast, Pal homologues display a distribution complementary to OmpM, being largely present in the Gracilicutes, while they are totally absent from the Terrabacteria (**Figure** 2, green dots). The distribution of OmpA is patchier (**Figure 2**, dark violet dots), but it also concentrates mainly in the Gracilicutes. Within Terrabacteria, we could only find OmpA homologues in some *Negativicutes* (including *V. parvula*), and in two candidate phyla (Margulisbacteria and

148 Wallbacteria/Riflebacteria), which were likely acquired via horizontal gene transfers
149 from the Gracilicutes (Supplementary Figure S1b). Finally, whereas Lpp is largely
150 considered as the textbook example of OM tethering, it is in fact restricted to a subclade
151 of *Gammaproteobacteria* (orders *Aeromonadales, Alteromonadales, Enterobacterales*, and
152 *Vibrionales*) (**Figure 2** and Supplementary Data Sheet 1E), extending recent analyses on
153 a much smaller taxonomic sampling [34,35].

154 These results highlight the existence of a major divide in how diderm bacteria
155 attach their OM, OmpM and Pal representing the main mechanisms in Terrabacteria
156 and Gracilicutes, respectively. Because Pal is a lipoprotein, its origin may be linked
157 with the emergence of the Lol system, the machinery delivering lipoproteins to the
158 OM [36]. Indeed, while the Lol system is widely distributed in the Gracilicutes, and
159 notably every time that Pal is present (**Figure 2**, orange dots, and Supplementary Data
160 Sheet 1A and B), we could not find any homologues of the components of the Lol
161 machinery in the Terrabacteria, with the exception of Deinococcus/Thermus (likely
162 acquired by horizontal gene transfer, Supplementary Figure S2).

163 Finally, because the few characterized OmpM-based tethers seem to all use
164 recognition between the SLH domain and pyruvylated secondary cell wall polymers
165 (the use of cadaverinated PG in the *Negativicutes* possibly being an exception, see
166 Supplementary Results and Discussion 1.4), we analyzed the distribution of
167 homologues of CsaB, the pyruvyl transferase that is responsible for the PG
168 modification, and of the SLH domains (Supplementary Data Sheet 1D). Indeed, CsaB
169 and SLH co-occur in most diderm Terrabacteria (**Figure 2**, lilac dots), extending what
170 previously noticed on a smaller taxonomic sample [37], and match closely the
171 distribution of OmpM, but are instead practically absent in the Gracilicutes. This

correlation strongly suggests that OM attachment to pyruvylated PG is a conserved feature of diderm Terrabacteria.

Deletion of OmpM in *V. parvula* leads to a striking phenotype

The presence of one major OM tethering system in the Terrabacteria may explain why there were multiple independent losses of the OM specifically in this clade (**Figure 2**). We therefore sought to investigate the consequences of perturbing OM attachment by deleting OmpM in the genetically tractable diderm Firmicute *Veillonella parvula*. The *V. parvula* SKV38 genome contains four OmpM coding genes, as well as a predicted gene coding for an OmpA homologue, but no Lpp or Pal homologues. We constructed a mutant of the three adjacent *ompM1* to *ompM3* genes (Δ*ompM1-3*), a mutant of the *ompM4* gene (Δ*ompM4*), which lies elsewhere in the genome, a quadruple deletion mutant (Δ*ompM1-4*), a mutant of *ompA* (Δ*ompA*) and a quintuple mutant (Δ*ompA*Δ*ompM1-4*). We could not obtain single gene mutants of the *ompM1-3* genes due to their very similar nucleotide sequences (Supplementary Figure S3), and the fact that the intergenic regions are equally similar.

With respect to the wild type, the Δ*ompM1-3* and Δ*ompM1-4* strains presented severe growth defects, and were extremely sensitive to sodium deoxycholate, EDTA, SDS, and vancomycin (**Figure 3a,** Extended Data Table ED1). On the contrary, the Δ*ompM4* and Δ*ompA* mutants were not affected (**Figure 3a,** Extended Data Table ED1). The quintuple Δ*ompA*Δ*ompM1-4* mutant had the strongest growth defect and sensitivity to stress (**Figure 3a,** Extended Data Table ED1). This may be linked to the fact that it lacks five of the six porins predicted in the genome (the sixth being FNLLGLLA_00833, not involved in OM attachment as it has no PG attachment

196 domain) likely impairing the uptake of nutrients and exchanges with the environment
197 rather than cell envelope organization.

198 Under light microscopy, the Δ*ompM1-3* mutants displayed very large vesicles,
199 with sizes ranging from a few hundred nanometers to ~8 μm in diameter (**Figure 3b**).
200 The quadruple (Δ*ompM1-4*) and quintuple (Δ*ompA*Δ*ompM1-4*) mutants presented a
201 phenotype similar to Δ*ompM1-3*, whereas the Δ*ompM4* and Δ*ompA* mutants were not
202 affected in cell morphology (**Figure 3b**). Finally, expression *in trans* of both native and
203 HA-tagged *ompM1*, whose homologue in *V. parvula* DSM2008 corresponds to the most
204 abundant outer membrane protein [27], almost completely reverted the mutant
205 phenotype (Extended Data Table ED1, Extended Data Figure ED2). However, this was
206 not the case of native or HA-tagged variants of the *ompA* and *ompM4* genes (Extended
207 Data Figure ED3). OmpM4 displays indeed specific differences in its SLH domain with
208 respect to OmpM1-3 proteins that may make it nonfunctional or less efficient
209 (Supplementary Figure S4 and Supplementary Results and Discussion 2).

210 Altogether, these results suggest that OmpM1-3 represent the main system
211 responsible for OM tethering in *V. parvula*, and that OmpA and OmpM4 have a less
212 important role, or even a different one, such as the exchange of nutrients or/and toxic
213 metabolic products with the environment via their porin component. We therefore
214 focused on further analysis of the triple Δ*ompM1-3* mutant.

215

216 **Ultrastructural details of the *V. parvula* Δ*ompM1-3* mutant**

217 High-resolution 3D Structured Illumination Microscopy (3D SIM) of the
218 Δ*ompM1-3* mutant revealed further its defects as compared to the WT (Figure 4). In the
219 mutant, the OM appeared substantially detached and formed very large vesicular
220 structures, within which cells appeared to continue dividing as shown by the presence

of multiple nucleoids (**Figure 4b** and **4c**). In contrast, the mutants complemented by expression of OmpM1 had a phenotype undistinguishable from the WT (**Figure 4a** and **4d**), whereas this was not the case in the absence of induction (**Figure 4e**). Finally, some vesicles appeared empty as devoid of any DNA signal (**Figure 4b**, white arrows and the inlet in **Figure 4e**).

Although the thickness of the frozen samples (~400-500 nm) was at the limit of observable objects by Cryo-ET, we obtained additional insights into the ultrastructural organization of the Δ*ompM1-3* mutant with respect to the WT (**Figure 5a-c**, Extended Data Figure ED4, Supplementary Movies S1-3). *V. parvula* WT cells are cocci with a perfectly visible diderm envelope (**Figure 5a**). In the Δ*ompM1-3* mutant, the cells conserved their coccus shape, and were surrounded by the IM and a contiguous layer of slightly but significatively thicker PG (15.7 ± 2.4 nm (n=30) as compared to 11.7 ± 1.8 nm (n=30) in the WT; $p<10^{-5}$ according to two-tailed Student's t test and permutation test for independent groups). However, the OM appeared vastly detached from the cell body, forming an enlarged, inflated periplasm with a higher density than the surrounding medium (suggesting the presence of normal proteinaceous periplasmic components), shared by numerous dividing cells (**Figure 5b** and **5c**, Extended Data Figure ED4, Supplementary Movies S2 and S3). The inner diameter of the cells was 549 ± 46 nm (n=37), not significantly different from the WT (560 ± 37 nm (n=37)) according to two-tailed Student's test and permutation test for independent groups. Consistent with the 3D-SIM images, cells within the vesicles displayed partial attachment to the OM, possibly helped by the presence of envelope-spanning machineries (see also Supplementary Results and Discussion 3). In some cases, the vesicles also contained degraded cells with patches of IM still attached to the OM (**Figure 5b**, yellow asterisk). Most of the large vesicles were connected by pearling

OM tubes that could reach a few tenths of microns in length, probably remnants of budding vesicles (**Figure 5b**, white arrows). In some of the samples embedded in thinner ice, even surface pili or fimbriae still linked to the detached OM could be visualized (**Figure 5b** and Extended Data Figure ED4, pink arrows). Strikingly, the strong phenotype of the Δ*ompM1-3* could be totally rescued by *in trans* expression of *ompM1*, indicating that a single OmpM manages to restore OM tethering (**Figure 5d**, Supplementary Movie S4).

Discussion

Our results reveal an ancient divide in the systems involved in OM stability in Bacteria and suggest a plausible scenario for their origin and evolution. Current evidence points to a common ancestor of all Bacteria that already possessed a complex diderm cell envelope [1,3,4]. This implies that it would have needed an OM tether. Our results suggest that Pal and Lpp emerged within the Gracilicutes, whereas OmpM and OmpA appear to be the most ancient OM tethers, being present in deep branches of the Terrabacteria and Gracilicutes, respectively (**Figure 2**). Two possible scenarios can be put forward for the origin and evolution of OmpM and OmpA (**Figure 6**). In the first scenario, OmpM would represent a simple system that was already present in the Last Bacterial Common Ancestor (LBCA) (**Figure 6**, scenario 1) allowing OM tethering while at the same time fulfilling a generalist porin function of diffusion through the membrane, as shown experimentally for the OmpM of the Negativicute *S. ruminantium* [38] and for Slp of *D. radiodurans* [39]. This ancestral OmpM system would have been inherited in the branch leading to present day Terrabacteria and replaced in the branch leading to Gracilicutes by OmpA, followed by the progressive appearance of the other multiple redundant systems (Pal, Lpp). OmpA may represent a possible transition

state in this scenario, as it is the only system present in Fusobacteria and Spirochaetes, two phyla at the interface between Terrabacteria and Gracilicutes (**Figure 2**). OmpA would have replaced OmpM by still being able to use its integral OM beta barrel to attach to the OM but switching its PG attachment from the SLH domain to an OmpA domain. This change in interaction would have made dispensable in the Gracilicutes the specific PG modifications (secondary cell wall polymers or cadaverine) needed for SLH domain binding by OmpM in diderm Terrabacteria. An alternative scenario (**Figure 6**, scenario 2) would place OmpA as the ancestral OM tethering system in the LCBA. In this case, OmpA would have been replaced by an OmpM-based system in the lineage leading to Terrabacteria following the appearance of pyruvylation of secondary cell wall polymers by CsaB and of SLH domains capable of recognizing it. As an alternative to these two scenarios, it cannot be excluded that both OmpM and OmpA were ancestrally present and were later independently lost in the lineage leading to the Gracilicutes or the Terrabacteria, respectively, or even that the LBCA had a completely different type of OM tether.

In all scenarios, the appearance of multiple OM tethering systems in the Gracilicutes would have followed the same path (**Figure 6**). It is likely that Pal originated from OmpA, as suggested by the fact that they share the same domain to attach to PG and differ only by the mechanism of attachment to the OM. To be inserted correctly into the OM, Pal needs the Lol machinery and could have therefore only have appeared after – or in concomitance with – the emergence of this system. It may be argued that OM lipoproteins were already present in the LBCA and were exported and inserted by another, yet unknown mechanism, which would have been inherited in the Terrabacteria but replaced by Lol in the Gracilicutes. However, a few arguments weaken this hypothesis. There is currently no experimental evidence for the presence

296 of OM lipoproteins in members of the Terrabacteria, to the exception of
297 Deinococcus/Thermus, which in fact acquired a Lol system secondarily via horizontal
298 gene transfer from the Gracilicutes (Supplementary Figure S2). The report of OM
299 lipoproteins in Cyanobacteria[40] is unclear, as admitted by the authors, because all the
300 lipoproteins found in the OM preparations were also found in the IM preparations,
301 and all but one also in the thylakoid membrane preparations. In addition, the study of
302 the *V. parvula* proteome found the presence of lipoproteins in the IM but not the OM
303 [27]. Finally, the absence of OM lipoproteins in the Terrabacteria would also be consistent
304 with the fact that the major machineries for OM biosynthesis such as Bam and Lpt lack
305 specifically in this clade the OM lipoprotein components found in the Gracilicutes ([41–
306 [43] and personal observations).
307 The reasons for takeover of OM tethering by multiple redundant systems in the
308 Gracilicutes are unclear. The apparent much larger diversification of the Gracilicutes
309 with respect to the Terrabacteria (**Figure 2**) suggests that this may have been
310 advantageous, for instance by providing a stronger attachment allowing higher
311 resistance to stress on the OM. This tight tethering could be the reason why no loss of
312 the OM ever occurred in the Gracilicutes. It is true that not all Gracilicutes have
313 redundant systems, with some members appearing to possess only Pal (**Figure 2**). It is
314 possible that Pal provides alone a strong tether in these species, but also it is not
315 excluded that they have additional alternative systems. Indeed, two completely novel
316 OM attachment systems have been recently described in Proteobacteria involving
317 porins[44–46]: a two component system in which a periplasmic protein PapA attaches both
318 to the peptidoglycan and to the integral outer membrane beta barrel protein OmpC,
319 common in *Betaproteobacteria*[46], and numerous beta barrel outer membrane proteins

covalently attached to the peptidoglycan in *Alphaproteobacteria* but also in some *Gammaproteobacteria*[44,45].

The situation is strikingly different in the Terrabacteria, which show more variability of cell envelopes, and where multiple independent losses of the OM can be inferred, at least at the divergence of three large clades of monoderms (Actinobacteria, Chloroflexi, and CPR), and multiple times within the Firmicutes (**Figure 2**). It is tempting to speculate that these multiple OM losses are linked to the presence of only a single main OM attachment represented by OmpM, which could have made members of Terrabacteria somehow more permissive to cell envelope perturbation. The state observed in Thermotogae, where the OM is largely detached at the cell poles[33], as well as the rotund bodies (where one OM surrounds multiple cells) observed in Dictyoglomi and Deinococcus/Thermus[47,48] might testify to such higher instability.

We propose that inactivation of OmpM may have been one the evolutionary mechanisms for loss of the OM and the emergence of monoderms from diderms. The mechanistic details of this transition are currently unclear. Increase in PG thickness to compensate for OM instability may have been an important step, similarly to what we observed in our *V. parvula* Δ*ompM1-3* mutant. Whether this increase is a mechanical consequence of the space left by a larger periplasm and/or a reaction to cell envelope stress caused by OM detachment remains to be determined. It may be also wondered if vestiges of the OmpM system were maintained after OM loss. From our analysis it appears that transition to the monoderm cell envelope was often accompanied not only by loss of the porins but also the SLH domains, together with the CsaB enzyme allowing the PG modification necessary for their attachment (**Figure 2**). In some monoderm lineages, the SLH/CsaB system was kept and possibly repurposed for

345 other functions. Functional repurposing is clearly visible in the Firmicutes, where the
346 SLH/CsaB system was largely kept, despite the multiple losses of the OM (see
347 Supplementary Results and Discussion 5).

348 Our results clearly demonstrate that OmpM and Pal can be considered as
349 markers of either diderm Terrabacteria or Gracilicutes, respectively. As such, their
350 presence in newly reconstructed genomes from uncultured bacterial lineages may
351 facilitate their taxonomic assignment. Moreover, their presence/absence may be used
352 to infer a diderm or monoderm phenotype in the vast majority of phyla for which cell
353 envelope characterization is missing. For example, the absence of OmpM from the
354 Chloroflexi favors the hypothesis that the diderm-like envelopes recently observed in
355 members of this phylum may actually be other types of structures [49].

356 The lack of any predicted OM attachment system in some diderm genomes
357 (**Figure 2**) is intriguing. While this can be explained by genome incompleteness in
358 uncultured candidate phyla, the specific case of Planctomycetes is particularly
359 interesting. Members of this phylum have an atypical diderm cell envelope and for a
360 long time were believed to lack peptidoglycan [50]. Their cell membrane is also unusually
361 dynamic, thanks to the presence of membrane coat proteins of eukaryotic type [51]. It is
362 possible that due to these particularities, they either evolved a novel attachment
363 system, or modified so profoundly the one inherited from their ancestor that it cannot
364 be recognized anymore.

365 Finally, our study highlights the genetically amenable diderm Firmicutes *V.*
366 *parvula* as an ideal new experimental model with respect to more classical Gracilicutes
367 models such as *E. coli*, which have an arsenal of – mostly non-essential – tethering
368 systems and where no similarly dramatic phenotypes arising from OM perturbation
369 have been observed. Further study of *V. parvula* will therefore allow a better

370 understanding of the multiple processes involved in the biogenesis of the diderm cell
371 envelope, and the mechanisms employed for maintaining OM integrity, an area of
372 intense interest in the fight of bacterial pathogens. Finally, the *V. parvula* OM
373 attachment mutant described in this work opens the way to further experimental work
374 that may allow to recapitulate and study the diderm-to-monoderm transition in the
375 laboratory.
376

Methods

Sequence analysis

We assembled a databank of 1,093 genomes representing all bacterial phyla present at the National Center for Biotechnology (NCBI) as of April 2020. We selected three species per order for each phylum. The number of genomes per phylum therefore reflects their taxonomical diversity (for a list of taxa see Supplementary Data Sheet 1). We chose preferably genomes from reference species and the most complete assemblies. We then queried this databank for the presence of Lpp, Pal, OmpA, OmpM, as wells as for the Lol system and CsaB homologues. Total absences of a given homologue in a phylum was confirmed by checking all the genomes available in the NCBI.

To identify Lpp and CsaB homologues, we used HMMSEARCH from the HMMER 3.3.2 package [52], and screened the databank using the Pfam domains LPP (PF04728) and PS_pyruv_trans (PF04230) with the option --cut_ga, the gathering threshold assigned by curators and corresponding to the minimum score a sequence must attain in order to belong to the full alignment of a Pfam entry. We also searched for Lpp homologues in a specific databank of 1083 Proteobacteria including 394 genomes from *Gammaproteobacteria*.

For the Lol system, we started by searching LolA in the databank using the Pfam domain PF03548 and HMMSEARCH with the option --cut_ga. As it is known that in some taxa LolA might be absent while the other components are present, we also searched for the ABC transporters LolC, LolD and LolE in a reduced databank composed of genomes from 192 taxa representing 36 main bacterial phyla. The alignments of protein families PRK10814 (LolC), PRK11629 (LolD) and PRK11146

(LolE) were downloaded from NCBI (Conserved Domain Database). HMM profiles were build using HMMBUILD from the HMMER 3.3.2 package and used to query the reduced databank. Because ABC transporter subunits belong to large protein families, the results were curated manually using annotations, synteny, alignments and phylogeny. Results were pooled for the LolC/E components, as search outputs overlapped greatly, and only a clade within *Gammaproteobacteria* possessed these distinct two paralogs.

As OmpA and Pal homologues share the same OmpA domain (PF00691), a specific strategy was applied to distinguish them: we first searched for proteins containing the OmpA domain using HMMSEARCH and the --cut_ga option; the retrieved hits were then submitted to PRED-TMBB 2 analysis [53] to select those containing a beta barrel, and the positive matches were considered as OmpA proteins. As PRED-TMBB 2 generates many false positives, in case of doubt the presence of a beta barrel was confirmed or invalidated with BOCTOPUS2 [54]. OmpA homologues were also identified in the same way in a local database of 230 Firmicutes. To identify Pal homologues, we used MacSyFinder 1.0.5 [55] to investigate the immediate genetic context of OmpA-containing proteins for the presence of a TolB homologue using the Pfam domains TolB_N (PF04052), TolB_like (PF15869), WD40 (PF00400) and PD40 (PF07676).

OmpM were defined as proteins containing an SLH domain and a beta barrel porin. To find OmpM homologues, we therefore first screened our genome databank for the presence of proteins containing SLH domains (PF00395) with HMMSEARCH and the –cut_ga option. All the hits also containing a beta barrel were then identified by using PRED-TMBB 2 and BOCTOPUS2. In Thermotogae, Bipolaricaulota and Fraserbacteria, the SLH domain and the beta barrel are split into two adjacent proteins.

To detect this configuration, we screened the proteins with an SLH domain for the presence of neighboring beta barrel structures. Results were manually curated using alignment, functional annotation, protein domains and phylogeny.

Finally, the presence/absence of each OM attachment system was mapped onto a reference tree of Bacteria using custom made scripts and iTOL [56].

Phylogenetic analysis

To build the reference bacterial phylogeny, we assembled a smaller database of 377 genomes by selecting five taxa per phylum. We selected 15 representatives from the CPR and 46 from the Proteobacteria, as they are very diverse. Hidden Markov model (HMM)-based homology searches (with the option --cut_ga) were carried out with HMMSEARCH by using the pfam profiles PF04997.12, PF04998.17, PF04563.15, PF00562.28 and PF11987.8 corresponding to RNA polymerase subunits β, β′ and translation initiation factor IF-2. Single genes were aligned using MAFFT v7.407 with the L-INS-I option, and trimmed using BMGE-1.12 [57] with the BLOSUM30 substitution matrix. The resulting trimmed alignments were concatenated into a supermatrix (377 taxa and 2,206 amino acid positions). The ML tree was generated using IQ-TREE v.1.6.3 with the profile mixture model LG+C60+F+G, with ultrafast bootstrap supports calculated on 1,000 replicates of the original dataset. Curated OmpA homologues were aligned using MAFFT v7.407 with the L-INS-I option and the alignment trimmed with trimal with the option -gt 0.5. The tree was built using IQ-TREE with the best-fit model LG+F+G4 estimated by ModelFinder, and ultrafast bootstrap supports computed on 1000 replicates of the original dataset.

For the lol system analysis, curated LolD homologues were aligned using MAFFT v7.407 with the L-INS-I option and the alignment trimmed with BMGE-1.12

using BLOSUM30 replacement matrix. The tree was built using IQ-TREE with the best-fit model LG+G4+I+F estimated by ModelFinder, and ultrafast bootstrap supports computed on 1000 replicates of the original dataset. The same procedure was applied for curated LolCE homologues.

For the detailed analysis of the distribution of OmpM in the *Negativicutes*, we assembled a local database of 135 Negativicute proteomes, and we applied the same strategy as outlined above. Results were plotted onto a reference phylogenetic tree of *Negativicutes* based on a concatenation of translation initiation factor IF-2, and RNA polymerase subunits β and β' assembled as above. Sequences were aligned using MAFFT v7.407, trimmed using BMGE-1.12, concatenated (3027 amino acid positions per sequence in final alignment) and the tree was generated using IQ-TREE with the best fit LG+R5 model estimated by ModelFinder.

For the detailed analysis of the distribution of SLH domains and CsaB proteins in Firmicutes a local database of 230 Firmicutes was queried with HMMER 3.3.2 package using the HMM profiles for SLH (PF00395) and PS_pyruv_trans (PF04230) domains downloaded from pfam.xfam.org using the –cut_ga option.

Curated OmpM homologues (for OmpM-like proteins, we concatenated Ompα and Ompβ sequences) were aligned using MAFFT v7.407 [58] with the L-INS-I option and the alignment was trimmed by using trimal 1.4.22 [59] with the option -gt 0.7. The tree was built using IQ-TREE [60,61] with the best-fit model LG+F+R7 estimated by ModelFinder [61] according to the Bayesian information Criterion (BIC), and ultrafast bootstrap supports [62] computed on 1000 replicates of the original dataset.

Bacterial strains, culture conditions and strain manipulation

Bacterial strains used in this work are listed in Supplementary Table S1. *Escherichia coli* strains were genetically manipulated using standard laboratory procedures [63]. When needed, the following compounds were added to *E. coli* cultures at the following concentrations: ampicillin (liquid media) or ticarcillin (solid media) – 100 mg/l, chloramphenicol – 30 mg/l (liquid media) or 25 mg/l (solid media), apramycin – 50 mg/l, diaminopimelic acid – 300 μM, anhydrotetracycline – 250 μg/l.

V. parvula was manipulated as described previously [64,65], the culture media being either BHILC [65] or SK [64]. When needed, the following compounds were added to *V. parvula* cultures at the following concentrations: chloramphenicol – 25 mg/l, tetracycline – 9 mg/l, erythromycin – 200 mg/l, anhydrotetracycline – 250 μg/l. The anaerobic conditions were generated using the GenBag Anaer generator (Biomérieux), the C400M anaerobic chamber (Ruskinn) or the GP Campus anaerobic chamber (Jacomex). The anaerobic chambers were filled with a $H_2/CO_2/N_2$ (5%/5%/90%) mixture.

Plasmids, primers, and DNA manipulations

All plasmids and primers used in this study are listed in Supplementary Table S2 and S3, respectively. Clonings were performed using NEBuilder HiFi DNA Assembly Master Mix (New England Biolabs). Chemocompetent homemade *E. coli* DH5α cells [66] were used for transformation of cloning products or plasmids. *V. parvula* genomic DNA was extracted according to a protocol previously described for *Streptomyces* gDNA extraction [67] from stationary phase cultures in SK medium.

Conjugation between *E. coli* and *V. parvula*

We successfully developed a protocol for conjugative transfer of plasmids from *E. coli* to *V. parvula*, an important addition to the genetic toolbox to manipulate this bacterium. This was especially important when manipulating mutants that have lost their natural competence such as the Δ*ompM1-3* strain. The plasmid to conjugate was introduced into *E. coli* MFDpir strain by electrotransformation using standard protocol [68]. An overnight stationary culture was used to start a fresh culture by 1/100 dilution (180 rpm, 37°C, LB medium). When the culture reached OD_{600} comprised between 0.4 and 0.9, the cells were washed twice by an equal volume of LB, resuspended in 1/10 of initial volume and stored on ice upon further use. *V. parvula* cultures were launched from cells scratched from a SK petri dish in SK liquid medium at initial OD_{600} of 0.03 and grown anaerobically at 37°C until the OD reached 0.1 – 0.2. 0.5 ml of donor *E. coli* strain was mixed with 1 ml of acceptor *V. parvula* strain, centrifugated briefly, the excess volume of medium removed, and the resuspended cells were deposited in form of a droplet on an SK medium plate containing diaminopimelic acid. After 24h of anaerobic incubation at 37°C, the cells were scratched from the Petri dish, resuspended in SK medium and plated on selective SK medium without diaminopimelate.

Generation of *ompM* and *ompA* deletion mutants

The mutants were generated using the technique described previously [64]. Briefly, for *ompM4* and *ompA* deletion upstream and downstream fragments (about 1 kb in size) of the genes to delete as well as the chloramphenicol resistance cassette *catP* were amplified and assembled into one linear construct by PCR. For *ompM1-3* deletion, the tetracycline resistance cassette *tetM* was used. Moreover, as PCR assembly step proved difficult, the three fragments were cloned into the pUC18 *Xba*I site, and then the linear construct was obtained by PCR amplification. Natural competence allowed

to transform the SKV38 WT strain with the linear construct and induce homologous recombination (and subsequent gene replacement with the resistance marker), and the correct mutant construction was verified by PCR amplification (and sequencing of amplicons) of the recombination junction zones. The details of the constructions are given in Supplementary Information.

Generation of quadruple and quintuple mutants

To generate a quadruple Δ*ompM1-4* mutant, the Δ*ompM4* mutant was transformed with Δ*ompM1-3* gDNA according to previously established protocol [64]. The correctness of the mutant was verified by the PCR of the recombination junction zones, and by PCR verification of the absence of *ompM4* gene.

To generate a quintuple mutant, a novel linear construct was generated by PCR assembly, using upstream and downstream fragments (slightly below 1 kb in size) of the *ompA* gene, and the *ermE* resistance marker. This construct was used for transformation of the *ompM4* mutant according to previously established protocol [64], yielding a Δ*ompA*Δ*ompM4* strain, which was in turn transformed by the gDNA of the Δ*ompM1-3* strain, leading to the desired Δ*ompA*Δ*ompM1-4* strain. The correct mutant construction was verified by PCR amplification (and sequencing of amplicons) of the recombination junction zones as well as the absence of *ompA* and *ompM4* genes by PCR. The details of the constructions are given in Supplementary Information.

OmpM1, OmpM4 and OmpA Expression vector construction

The expression vectors were constructed by cloning the gene of interest with its native RBS or with a modified RBS into *Sac*I site of pRPF185 *Escherichia*/*Clostridium* conjugative shuttle tetracycline inducible expression vector [69]. In some vectors, an HA-

tag was added during the cloning process into a predicted extracellular loop of the beta barrel (the exact point of insertion of the HA-tag is presented for OmpM1 in the Supplementary Figure S5). The integrity of the constructs was verified by sequencing. The correct expression of HA-tagged protein was verified by Western Blot (Extended Data Figures ED3 and ED5a) and for OmpM1 also by immunomarking (Extended Data Figure ED5b and c). Additionally, the correct expression and addressing to the cell surface was also verified in *E. coli* (Extended Data Figure ED6). All vectors are described in the Supplementary Table S2, and all the details of the construction process are described in Supplementary Information.

Minimum inhibitory concentration (MIC) determination and growth curves

For MIC, serial twofold dilutions of sodium deoxycholate, EDTA, SDS and vancomycin were made in BHILC medium. The dilutions were put in 96-well flat bottom plates (150 μl per well). Bacterial strains to be tested were grown on SK plates (37°C, anaerobic conditions) for 2-3 days. They were scratched from the plate, resuspended in BHILC medium, and the OD_{600} was adjusted to 1.5. The wells were inoculated with 5 μl of bacterial suspension to obtain an initial OD_{600} of 0.05 and then incubated anaerobically at 37°C, 180 rpm for 24h. The MIC was defined as the lowest concentration at which the final OD was inferior to 0.1.

For growth curves, a 96-well flat bottom plate was filled with 250 μl per well of BHILC medium. The medium was partially degassed in -0.6 bar vacuum and preincubated 4h inside the GP Campus anaerobic chamber (Jacomex). Then, the wells were anaerobically seeded with 5 μl of the same bacterial suspension as for the MIC, as the OD in the well was 0.03. The plates were then sealed with Adhesive PCR Plate Seals (Thermo Fisher Scientific). The plates were then incubated in TECAN Sunrise

spectrophotometer for 24 hours at 37 °C. OD_{600} was measured every 30 minutes, after 15 min of orbital shaking. Each test was performed in pentaplicate.

Cultures for microscopy observation

For *V. parvula*, a liquid culture of 5 ml (in 50 ml Falcon tube) was launched from a glycerol stock in SK medium and incubated anaerobically at 37°C. For strains bearing no plasmid, the observations were made after two days of culture. Like the expression vector bearing strains, at the end of the second day the original culture was diluted 10x in fresh medium and incubated anaerobically overnight at 37°C either in presence or absence of anhydrotetracycline.

For *E. coli*, a liquid culture of 10 ml (in 50 ml Falcon tube) was launched from a glycerol stock in LB medium and incubated aerobically 24h at 37°C with 180 rpm rotative shaking. A new culture was launched by diluting the original culture 10x in fresh anhydrotetracycline containing medium and then incubated overnight in a 250 ml Erlenmeyer flask at 20°C with 180 rpm rotative shaking.

3D Structured Illumination Microscopy (3D SIM)

An aliquot of culture was mixed with FM 4-64 membrane staining dye (Thermo Fischer Scientific) at a final concentration of 5 mg/l and DAPI at a final concentration of 17 mg/l. Bacterial cell suspensions were applied on high precision coverslips (No. 1.5H, Sigma-Aldrich) coated with a solution of 0.01 % (w/v) of poly-L-lysine. After letting the cells attach onto the surface of the coverslip for 10 min, residual liquid was removed, 8 μL of antifade mounting medium (Vectashield) were applied and the coverslip was sealed to a slide. SIM was performed on a Zeiss LSM 780 Elyra PS1 microscope (Carl Zeiss, Germany) using C Plan-Apochromat 63× / 1.4 oil objective

with a 1.518 refractive index oil (Carl Zeiss, Germany). The samples were excited with laser at 405 nm for the DAPI staining and 561 nm for the FM4-64 staining and the emission was detected through emission filter BP 420-480 + LP 750 and BP 570-650 + LP 750, respectively. The fluorescence signal is detected on an EMCCD Andor Ixon 887 1 K camera. Raw images are composed of fifteen images per plane per channel (five phases, three angles), and acquired with a Z-distance of 0.10 µm. Acquisition parameters were adapted from one image to one other to optimize the signal to noise ratio. SIM images were processed with ZEN 2012 SP5 FP3 (black) software (Carl Zeiss, Germany) and then corrected for chromatic aberration using 100 nm TetraSpeck microspheres (ThermoFisher Scientific) embedded in the same mounting media as the sample. For further image analysis of SIM image z stacks we used Fiji (ImageJ) Version 2.0.0-rc-68/1.52i [70]. Namely, we assigned a color to the fluorescent channels, stacks were fused to a single image (z projection, maximum intensity) and brightness and contrast were slightly adapted. Regions of interest were cut out and, for uniformity, placed on a black squared background. Figures were compiled using Adobe Illustrator 2020 (Adobe Systems Inc. USA).

Cryogenic electron microscopy observation (CryoEM)

A solution of BSA-gold tracer (Aurion) containing 10-nm-diameter colloidal gold particles was added to a fresh culture of *V. parvula* with a final ratio of 3:1. A small amount of the sample was applied to the front (4 µl) and to the back (1.2 µl) of carbon-coated copper grids (Cu 200 mesh Quantifoil R2/2, Quantifoil, or Lacey, EMS), previously glow discharged 2 mA and 1.5-1.8x10^{-1} mbar for 1 min in an ELMO (Corduan) glow discharge system. The sample was then vitrified in a Leica EMGP system. Briefly, the excess liquid was removed by blotting with filter paper the back

side of the grids for 6-7 s at 18°C and 95% humidity, and then the sample was rapidly frozen by plunging it in liquid ethane. The grids were stored in liquid nitrogen until image acquisition in the TEM.

Cryo-electron microscopy was performed on a Tecnai 20 equipped with a field emission gun and operated at 200 kV (Thermo Fisher) using a Gatan 626 side entry cryoholder. Images were recorded using the SerialEM 3.7 beta software on a Falcon II (FEI, Thermo Fisher) direct electron detector, with a 14 μm pixel size. Digital images were acquired at nominal magnification of 29000x, corresponding to pixel size of 0.349 nm. For high-magnification images, the defocus was −8 μm. Cell width and peptidoglycan width were measured using Fiji [70]. Measurement of cell width was straightforward. For PG width, small sections (about 50 nm) of cell envelope images were excised, rotated so that envelope layers were vertical, and the Plot Profile tool was used to measure the width of the base of the peak corresponding to the PG layer. Dose-symmetric tilt series were collected on a 300kV Titan Krios (Thermo Fisher Scientific) transmission electron microscope equipped with a Quantum LS imaging filter (Gatan, with slit width of 20 eV), single-tilt axis holder and K3 direct electron detector (Gatan). Tilt series with an angular increment of 2° and an angular range of ±60° were acquired with the Tomography software (Thermo Fisher Scientific), version 5.2.0.5806REL. The total electron dose was 130 electrons per Å^2 at a pixel size of 8 Å. Dose symmetric tilt series were saved as separate stacks of frames and subsequently motion-corrected and re-stacked from −60° to +60° using IMOD's function align frames [71] with the help of a homemade bash script. Three-dimensional reconstructions were calculated in IMOD 4.9.10 by weighted back projection and a gaussian filter was used to enhance contrast and facilitate subsequent segmentation analysis. The 3D

segmentation of the tomograms was performed by using the Amira 2020.2 software (Thermo Fisher Scientific).

It should be noted that only a subpopulation of the triple mutant could be analyzed due to the frequent rupture of the fragile large vesicles during the blotting step of the sample preparation.

DATA AVAILABILITY STATEMENT

The authors declare that all data supporting the findings of this study are available within the paper and its supplementary information files (source data for figures 2, 3a, extended data figures 1, 2a, 3, 5a, 6a and supplementary data for supplementary figures S1a,b and S2a,b) or, otherwise, are available from the corresponding author upon request.

ACKNOWLEDGEMENTS

This work was supported by funding from the French National Research Agency (ANR) (Fir-OM ANR-16-CE12-0010), the Institut Pasteur "Programmes Transversaux de Recherche" (PTR 39-16), the French government's Investissement d'Avenir Program, Laboratoire d'Excellence "Integrative Biology of Emerging Infectious Diseases" (grant n°ANR-10-LABX-62-IBEID) and the Fondation pour la Recherche Médicale (grant DEQ20180339185). N.P. is funded by a Pasteur-Roux Postdoctoral Fellowship from the Institut Pasteur. We thank Alicia Jiménez-Fernández for help with *Veillonella* genetics techniques. We gratefully acknowledge the UTechS Photonic BioImaging (Imagopole), C2RT, Institut Pasteur (Paris, France) and the France–BioImaging infrastructure network supported by the French National Research Agency (ANR-10–INSB–04; Investments for the Future), and the Région Ile-de-France (program Domaine d'Intérêt Majeur-Malinf) for the use of the Zeiss LSM 780 Elyra PS1

microscope. We thank S. Tachon from the NanoImaging Core facility of the Center for Technological Resources and Research of Institut Pasteur for assistance with the tomography acquisitions at the Titan Krios microscope. We are grateful for equipment support from the French Government Programme Investissements d'Avenir France BioImaging (FBI, N° ANR-10-INSB-04-01). We thank M. Nilges and the Equipex CACSICE (Centre d'analyse de systèmes complexes dans les environnements complexes) for providing the Falcon II direct detector. The authors acknowledge the IT department at Institut Pasteur, Paris, for providing computational and storage services (TARS cluster).

AUTHORS CONTRIBUTIONS STATEMENT

JW performed all molecular biology and microbiology experiments with the assistance of TNT. ASR and JW performed the electron microscopy data acquisition, reconstructions and visualizations. NP performed the 3D-SIM data acquisition and treatment and drew the schematic representations (Figures 1 and 6). NT and JW performed the bioinformatic and evolutionary analysis. DP performed preliminary bioinformatic analyses in an early version of the manuscript. JMG provided lab facilities. CB and SG supervised the study. JW, CB and SG wrote the paper with contributions from ASR, NT, NP, and JMG. All authors contributed to the final version of the manuscript.

COMPETING INTEREST STATEMENT

All the authors declare that they have no competing interests

FIGURE LEGENDS

Figure 1. Schematic representation of the four major mechanisms for OM attachment to the cell wall: (**a**) Lpp, Pal and OmpA as the canonical *E. coli* systems, and OmpM as an alternative system reported from some Terrabacteria; (**b**) domain organization of the corresponding proteins. LPS means lipopolysaccharide, OM – outer membrane, PG – peptidoglycan, SS – signal sequence.

Figure 2. Distribution of major known OM attachment systems mapped on a reference phylogeny of Bacteria (a) and on a schematic tree of the Firmicutes (b). The phylogeny is based on the concatenation of RNA polymerase subunits β, β' and elongation factor IF-2 (2,206 amino-acid positions and 377 taxa) and is rooted in between the two large clades of the Terrabacteria and Gracilicutes, according to [4,72]. The tree was calculated using IQ-TREE version 1.6.3 with the model LG+C60+F+G and black dots indicate bootstrap values >90%. The presence of each of the four main attachment systems, of the Lol system, and of CsaB/SLH is marked with a colored dot. Arrows indicate the possible origin of each system. Red cross indicates the OM loss. The question mark in the LBCA indicates uncertainty on the presence of OmpM or OmpA (or yet another mechanism) (see Figure 6). Note that D indicates the presence of a classical OM (with or without LPS) as inferred either by experimental data or by the presence of Bam and other known OM systems. For this reason, Actinobacteria are marked as monoderms (M) even if some members have an OM made of mycolic acids, which is of more recent origin. In parentheses are indicated the number of genomes analyzed. All accession numbers are given in Supplementary Data Sheet 1A and 1B. The phylogenetic tree is available as a Newick file (Source Data for Figure 2.newick).

Figure 3. Phenotype of different *V. parvula* mutants generated in this study as compared to the WT. (a) – Growth curves. All data points represent the mean of a pentaplicate, error bars were omitted for sake of visibility. Cultures were made in BHILC medium in 96-well plates at 37°C under anaerobic conditions. **(b)** – Epifluorescence observation of cells labelled with the biological membrane staining dye FM 4-64 (Thermo Fisher Scientific). All scale bars represent 5 μm. The samples shown are representative of multiple (n>10) experiments.

Figure 4. Membrane and DNA staining of representative *V. parvula* WT and Δ*ompM1-3* mutant cells imaged by 3D SIM. Cell membranes were stained with by FM4-64 (red) and the DNA by DAPI (blue). (**a**) *V. parvula* WT. (**b** and **c**) Δ*ompM1-3* mutant of *V. parvula;* the panel (**b**) presents a large field of view where arrows indicate vesicles of different sizes devoid of any DNA signal. (**d**) Δ*ompM1-3* mutant of *V. parvula* complemented with pJW35 vector expressing OmpM1-HA under control of a *tet* promoter, induced overnight with 250 μg/l of anhydrotetracycline (+ATC). (**e**) Δ*ompM1-3* mutant of *V. parvula* complemented with an uninduced pJW35 vector (-ATC). Inlet shows membrane vesicles without DNA content. Scale bar in all images is 1 μm. The 3D-SIM acquisition was performed once, but the phenotype of the shown samples, as assessed by conventional fluorescence microscopy, is representative of multiple (n>20) experiments.

Figure 5. Cryo-electron tomography of *V. parvula* WT and mutant cells. (a) – WT, **(b-c)** – Δ*ompM1-3* mutant; detached outer membrane forming blebs and vesicles is well visible, **(d)** - Δ*ompM1*-3 mutant of *V. parvula* complemented with pJW35 vector (expressing OmpM1-HA under control of *tet* promoter) induced overnight with 250

751 μg/l of anhydrotetracycline. Left panels represent a sum of 10 tomogram slices (16
752 nm), right panels a 3D rendering of the cell envelope structure based on manual
753 segmentation of tomogram slices, middle panels are the superposition of a tomogram
754 slice and the 3D rendering. OM / blue marking – outer membrane, PG / red marking
755 – peptidoglycan, IM / green marking – inner membrane. White arrows show OM
756 tubules. Pink arrows show a bundle of fimbriae-like structures connecting two OM.
757 Yellow asterisk shows a degraded cell. Cyan arrows show bacteriophages (see
758 Supplementary Results and Discussion 4). All scale bars represent 0.5 μm. Videos
759 corresponding to panels a to d, containing all slices of the 3D tomogram reconstruction
760 are available as Supplementary Movies S1 to S4. The CryoEM acquisition was
761 performed twice, but the phenotype of the presented samples, as assessed by
762 conventional fluorescence microscopy, is representative of multiple (n>20)
763 experiments. The presence of phages, as visible in some Cryo-ET images, is not
764 responsible for the observed phenotypes (see Supplementary Discussion).
765
766 **Figure 6. Two scenarios of evolution of OM tethering in Bacteria.** Acquisitions are
767 marked with full line arrows, and losses with dotted line arrows. In scenario 1, the
768 LBCA tethered its OM via OmpM, and through interaction of the SLH domain with
769 secondary cell wall polymers (SCWP) pyruvylated by the CsaB enzyme; this cell
770 envelope configuration was inherited in diderm Terrabacteria, whereas in Gracilicutes
771 the SLH domain was replaced by an OmpA domain leading to the OmpA tethering
772 system, and the pyruvylated secondary cell wall polymers were lost along with CsaB.
773 In scenario 2, the LBCA tethered its OM via OmpA; in Terrabacteria, the OmpA
774 domain was replaced by the SLH domain upon appearance of the CsaB enzyme
775 pyruvylating the SCWP, leading to the OmpM tethering system, whereas OmpA was

conserved in Gracilicutes. In both scenarios, Pal arose from OmpA by replacement of the porin domain with a lipid tail upon appearance of the Lol system to address lipoproteins to the OM. Finally, Lpp appeared *de novo* within *Gammaproteobacteria*.

References

1. Megrian, D., Taib, N., Witwinowski, J., Beloin, C. & Gribaldo, S. One or two membranes? Diderm Firmicutes challenge the Gram-positive/Gram-negative divide. *Mol. Microbiol.* **113**, 659–671 (2020).
2. Tocheva, E. I., Ortega, D. R. & Jensen, G. J. Sporulation, bacterial cell envelopes and the origin of life. *Nat. Rev. Microbiol.* **14**, 535–542 (2016).
3. Taib, N. *et al.* Genome-wide analysis of the Firmicutes illuminates the diderm/monoderm transition. *Nat. Ecol. Evol.* **4**, 1661–1672 (2020).
4. Coleman, G. A. *et al.* A rooted phylogeny resolves early bacterial evolution. *Science* **372**, (2021).
5. Cavalier-Smith, T. The neomuran origin of archaebacteria, the negibacterial root of the universal tree and bacterial megaclassification. *Int. J. Syst. Evol. Microbiol.* **52**, 7–76 (2002).
6. Braun, V. & Rehn, K. Chemical characterization, spatial distribution and function of a lipoprotein (murein-lipoprotein) of the E. coli cell wall. The specific effect of trypsin on the membrane structure. *Eur. J. Biochem.* **10**, 426–438 (1969).
7. Braun, V. Covalent lipoprotein from the outer membrane of Escherichia coli. *Biochim. Biophys. Acta* **415**, 335–377 (1975).
8. Suzuki, H. *et al.* Murein-lipoprotein of Escherichia coli: a protein involved in the stabilization of bacterial cell envelope. *Mol. Gen. Genet. MGG* **167**, 1–9 (1978).
9. Yem, D. W. & Wu, H. C. Physiological characterization of an Escherichia coli mutant altered in the structure of murein lipoprotein. *J. Bacteriol.* **133**, 1419–1426 (1978).
10. Cascales, E., Bernadac, A., Gavioli, M., Lazzaroni, J.-C. & Lloubes, R. Pal lipoprotein of Escherichia coli plays a major role in outer membrane integrity. *J. Bacteriol.* **184**, 754–759 (2002).
11. Cohen, E. J., Ferreira, J. L., Ladinsky, M. S., Beeby, M. & Hughes, K. T. Nanoscale-length control of the flagellar driveshaft requires hitting the tethered outer membrane. *Science* **356**, 197–200 (2017).
12. Bouveret, E., Bénédetti, H., Rigal, A., Loret, E. & Lazdunski, C. In vitro characterization of peptidoglycan-associated lipoprotein (PAL)-peptidoglycan and PAL-TolB interactions. *J. Bacteriol.* **181**, 6306–6311 (1999).
13. Parsons, L. M., Lin, F. & Orban, J. Peptidoglycan recognition by Pal, an outer membrane lipoprotein. *Biochemistry* **45**, 2122–2128 (2006).
14. Bernadac, A., Gavioli, M., Lazzaroni, J. C., Raina, S. & Lloubès, R. Escherichia coli tol-pal mutants form outer membrane vesicles. *J. Bacteriol.* **180**, 4872–4878 (1998).
15. Gerding, M. A., Ogata, Y., Pecora, N. D., Niki, H. & de Boer, P. A. J. The trans-envelope Tol-Pal complex is part of the cell division machinery and required for proper outer-membrane invagination during cell constriction in E. coli. *Mol. Microbiol.* **63**, 1008–1025 (2007).
16. Szczepaniak, J., Press, C. & Kleanthous, C. The multifarious roles of Tol-Pal in Gram-

820 negative bacteria. *FEMS Microbiol. Rev.* **44**, 490–506 (2020).
821 17. Park, J. S. *et al.* Mechanism of anchoring of OmpA protein to the cell wall
822 peptidoglycan of the gram-negative bacterial outer membrane. *FASEB J. Off. Publ. Fed. Am.*
823 *Soc. Exp. Biol.* **26**, 219–228 (2012).
824 18. Samsudin, F., Boags, A., Piggot, T. J. & Khalid, S. Braun's Lipoprotein Facilitates
825 OmpA Interaction with the Escherichia coli Cell Wall. *Biophys. J.* **113**, 1496–1504 (2017).
826 19. Tocheva, E. I. *et al.* Peptidoglycan remodeling and conversion of an inner membrane
827 into an outer membrane during sporulation. *Cell* **146**, 799–812 (2011).
828 20. Antunes, L. C. *et al.* Phylogenomic analysis supports the ancestral presence of LPS-
829 outer membranes in the Firmicutes. *eLife* **5**, (2016).
830 21. Kamio, Y. & Takahashi, H. Outer membrane proteins and cell surface structure of
831 Selenomonas ruminantium. *J. Bacteriol.* **141**, 899–907 (1980).
832 22. Kalmokoff, M. L. *et al.* Physical and genetic characterization of an outer-membrane
833 protein (OmpM1) containing an N-terminal S-layer-like homology domain from the
834 phylogenetically Gram-positive gut anaerobe Mitsuokella multacida. *Anaerobe* **15**, 74–81
835 (2009).
836 23. Kojima, S. *et al.* Cadaverine covalently linked to peptidoglycan is required for
837 interaction between the peptidoglycan and the periplasm-exposed S-layer-homologous
838 domain of major outer membrane protein Mep45 in Selenomonas ruminantium. *J. Bacteriol.*
839 **192**, 5953–5961 (2010).
840 24. Kojima, S. & Kamio, Y. Molecular basis for the maintenance of envelope integrity in
841 Selenomonas ruminantium: cadaverine biosynthesis and covalent modification into the
842 peptidoglycan play a major role. *J. Nutr. Sci. Vitaminol. (Tokyo)* **58**, 153–160 (2012).
843 25. Kamio, Y., Itoh, Y. & Terawaki, Y. Chemical structure of peptidoglycan in
844 Selenomonas ruminantium: cadaverine links covalently to the D-glutamic acid residue of
845 peptidoglycan. *J. Bacteriol.* **146**, 49–53 (1981).
846 26. Kamio, Y. & Nakamura, K. Putrescine and cadaverine are constituents of
847 peptidoglycan in Veillonella alcalescens and Veillonella parvula. *J. Bacteriol.* **169**, 2881–
848 2884 (1987).
849 27. Poppleton, D. I. *et al.* Outer Membrane Proteome of Veillonella parvula: A Diderm
850 Firmicute of the Human Microbiome. *Front. Microbiol.* **8**, 1215 (2017).
851 28. Hansel, A. & Tadros, M. H. Characterization of two pore-forming proteins isolated
852 from the outer membrane of Synechococcus PCC 6301. *Curr. Microbiol.* **36**, 321–326 (1998).
853 29. Kojima, S. & Okumura, Y. Outer membrane-deprived cyanobacteria liberate
854 periplasmic and thylakoid luminal components that support the growth of heterotrophs.
855 *bioRxiv* 2020.03.24.006684 (2020) doi:10.1101/2020.03.24.006684.
856 30. Fernández-Herrero, L. A., Olabarría, G., Castón, J. R., Lasa, I. & Berenguer, J.
857 Horizontal transference of S-layer genes within Thermus thermophilus. *J. Bacteriol.* **177**,
858 5460–5466 (1995).
859 31. Olabarría, G., Carrascosa, J. L., de Pedro, M. A. & Berenguer, J. A conserved motif in
860 S-layer proteins is involved in peptidoglycan binding in Thermus thermophilus. *J. Bacteriol.*
861 **178**, 4765–4772 (1996).
862 32. Cava, F., de Pedro, M. A., Schwarz, H., Henne, A. & Berenguer, J. Binding to
863 pyruvylated compounds as an ancestral mechanism to anchor the outer envelope in primitive
864 bacteria. *Mol. Microbiol.* **52**, 677–690 (2004).
865 33. Engel, A. M., Cejka, Z., Lupas, A., Lottspeich, F. & Baumeister, W. Isolation and
866 cloning of Omp alpha, a coiled-coil protein spanning the periplasmic space of the ancestral
867 eubacterium Thermotoga maritima. *EMBO J.* **11**, 4369–4378 (1992).

34. Egan, A. J. F. Bacterial outer membrane constriction. *Mol. Microbiol.* **107**, 676–687 (2018).
35. Asmar, A. T. & Collet, J.-F. Lpp, the Braun lipoprotein, turns 50—major achievements and remaining issues. *FEMS Microbiol. Lett.* **365**, (2018).
36. Braun, V. & Hantke, K. Lipoproteins: Structure, Function, Biosynthesis. *Subcell. Biochem.* **92**, 39–77 (2019).
37. Mesnage, S. *et al.* Bacterial SLH domain proteins are non-covalently anchored to the cell surface via a conserved mechanism involving wall polysaccharide pyruvylation. *EMBO J.* **19**, 4473–4484 (2000).
38. Kojima, S. *et al.* Peptidoglycan-associated outer membrane protein Mep45 of rumen anaerobe Selenomonas ruminantium forms a non-specific diffusion pore via its C-terminal transmembrane domain. *Biosci. Biotechnol. Biochem.* **80**, 1954–1959 (2016).
39. Farci, D. *et al.* Structural insights into the main S-layer unit of Deinococcus radiodurans reveal a massive protein complex with porin-like features. *J. Biol. Chem.* **295**, 4224–4236 (2020).
40. Pisareva, T. *et al.* Model for Membrane Organization and Protein Sorting in the Cyanobacterium Synechocystis sp. PCC 6803 Inferred from Proteomics and Multivariate Sequence Analyses. *J. Proteome Res.* **10**, 3617–3631 (2011).
41. Heinz, E., Selkrig, J., Belousoff, M. J. & Lithgow, T. Evolution of the Translocation and Assembly Module (TAM). *Genome Biol. Evol.* **7**, 1628–1643 (2015).
42. Webb, C. T., Heinz, E. & Lithgow, T. Evolution of the β-barrel assembly machinery. *Trends Microbiol.* **20**, 612–620 (2012).
43. Anwari, K. *et al.* The evolution of new lipoprotein subunits of the bacterial outer membrane BAM complex. *Mol. Microbiol.* **84**, 832–844 (2012).
44. Godessart, P. *et al.* β-Barrels covalently link peptidoglycan and the outer membrane in the α-proteobacterium Brucella abortus. *Nat. Microbiol.* **6**, 27–33 (2021).
45. Sandoz, K. M. *et al.* β-Barrel proteins tether the outer membrane in many Gram-negative bacteria. *Nat. Microbiol.* **6**, 19–26 (2021).
46. Wang, Y.-H. *et al.* PapA, a peptidoglycan-associated protein, interacts with OmpC and maintains cell envelope integrity. *Environ. Microbiol.* **23**, 600–612 (2021).
47. Hoppert, M. *et al.* Structure–functional analysis of the Dictyoglomus cell envelope. *Syst. Appl. Microbiol.* **35**, 279–290 (2012).
48. Brock, T. D. & Edwards, M. R. Fine structure of Thermus aquaticus, an extreme thermophile. *J. Bacteriol.* **104**, 509–517 (1970).
49. Gaisin, V. A., Kooger, R., Grouzdev, D. S., Gorlenko, V. M. & Pilhofer, M. Cryo-Electron Tomography Reveals the Complex Ultrastructural Organization of Multicellular Filamentous Chloroflexota (Chloroflexi) Bacteria. *Front. Microbiol.* **11**, 1373 (2020).
50. van Teeseling, M. C. F. *et al.* Anammox Planctomycetes have a peptidoglycan cell wall. *Nat. Commun.* **6**, 6878 (2015).
51. Boedeker, C. *et al.* Determining the bacterial cell biology of Planctomycetes. *Nat. Commun.* **8**, 14853 (2017).
52. Johnson, L. S., Eddy, S. R. & Portugaly, E. Hidden Markov model speed heuristic and iterative HMM search procedure. *BMC Bioinformatics* **11**, 431 (2010).
53. Tsirigos, K. D., Elofsson, A. & Bagos, P. G. PRED-TMBB2: improved topology prediction and detection of beta-barrel outer membrane proteins. *Bioinforma. Oxf. Engl.* **32**, i665–i671 (2016).
54. Hayat, S., Peters, C., Shu, N., Tsirigos, K. D. & Elofsson, A. Inclusion of dyad-repeat pattern improves topology prediction of transmembrane β-barrel proteins. *Bioinforma. Oxf.*

Engl. **32**, 1571–1573 (2016).
55. Abby, S. S., Néron, B., Ménager, H., Touchon, M. & Rocha, E. P. C. MacSyFinder: A Program to Mine Genomes for Molecular Systems with an Application to CRISPR-Cas Systems. *PLOS ONE* **9**, e110726 (2014).
56. Letunic, I. & Bork, P. Interactive Tree Of Life (iTOL) v4: recent updates and new developments. *Nucleic Acids Res.* **47**, W256–W259 (2019).
57. Criscuolo, A. & Gribaldo, S. BMGE (Block Mapping and Gathering with Entropy): a new software for selection of phylogenetic informative regions from multiple sequence alignments. *BMC Evol. Biol.* **10**, 210 (2010).
58. Katoh, K. & Standley, D. M. MAFFT multiple sequence alignment software version 7: improvements in performance and usability. *Mol. Biol. Evol.* **30**, 772–780 (2013).
59. Capella-Gutiérrez, S., Silla-Martínez, J. M. & Gabaldón, T. trimAl: a tool for automated alignment trimming in large-scale phylogenetic analyses. *Bioinforma. Oxf. Engl.* **25**, 1972–1973 (2009).
60. Nguyen, L.-T., Schmidt, H. A., von Haeseler, A. & Minh, B. Q. IQ-TREE: a fast and effective stochastic algorithm for estimating maximum-likelihood phylogenies. *Mol. Biol. Evol.* **32**, 268–274 (2015).
61. Kalyaanamoorthy, S., Minh, B. Q., Wong, T. K. F., von Haeseler, A. & Jermiin, L. S. ModelFinder: fast model selection for accurate phylogenetic estimates. *Nat. Methods* **14**, 587–589 (2017).
62. Hoang, D. T., Chernomor, O., von Haeseler, A., Minh, B. Q. & Vinh, L. S. UFBoot2: Improving the Ultrafast Bootstrap Approximation. *Mol. Biol. Evol.* **35**, 518–522 (2018).
63. Green, M. R. & Sambrook, J. *Molecular Cloning: A Laboratory Manual.* (Cold Spring Harbor Laboratory Press., 2012).
64. Knapp, S. *et al.* Natural Competence Is Common among Clinical Isolates of Veillonella parvula and Is Useful for Genetic Manipulation of This Key Member of the Oral Microbiome. *Front. Cell. Infect. Microbiol.* **7**, 139 (2017).
65. Béchon, N. *et al.* Autotransporters Drive Biofilm Formation and Autoaggregation in the Diderm Firmicute Veillonella parvula. *J. Bacteriol.* **202**, (2020).
66. Inoue, H., Nojima, H. & Okayama, H. High efficiency transformation of Escherichia coli with plasmids. *Gene* **96**, 23–28 (1990).
67. Jacques, I. B. *et al.* Analysis of 51 cyclodipeptide synthases reveals the basis for substrate specificity. *Nat. Chem. Biol.* **11**, 721–727 (2015).
68. Robey, R. B., Sharma, R. C. & Schimke, R. T. Preparation of electrocompetent E. coli using salt-free growth medium. *BioTechniques* **20**, 42–44 (1996).
69. Fagan, R. P. & Fairweather, N. F. Clostridium difficile has two parallel and essential Sec secretion systems. *J. Biol. Chem.* **286**, 27483–27493 (2011).
70. Schindelin, J. *et al.* Fiji: an open-source platform for biological-image analysis. *Nat. Methods* **9**, 676–682 (2012).
71. Mastronarde, D. N. & Held, S. R. Automated tilt series alignment and tomographic reconstruction in IMOD. *J. Struct. Biol.* **197**, 102–113 (2017).
72. Raymann, K., Brochier-Armanet, C. & Gribaldo, S. The two-domain tree of life is linked to a new root for the Archaea. *Proc. Natl. Acad. Sci. U. S. A.* **112**, 6670–6675 (2015).

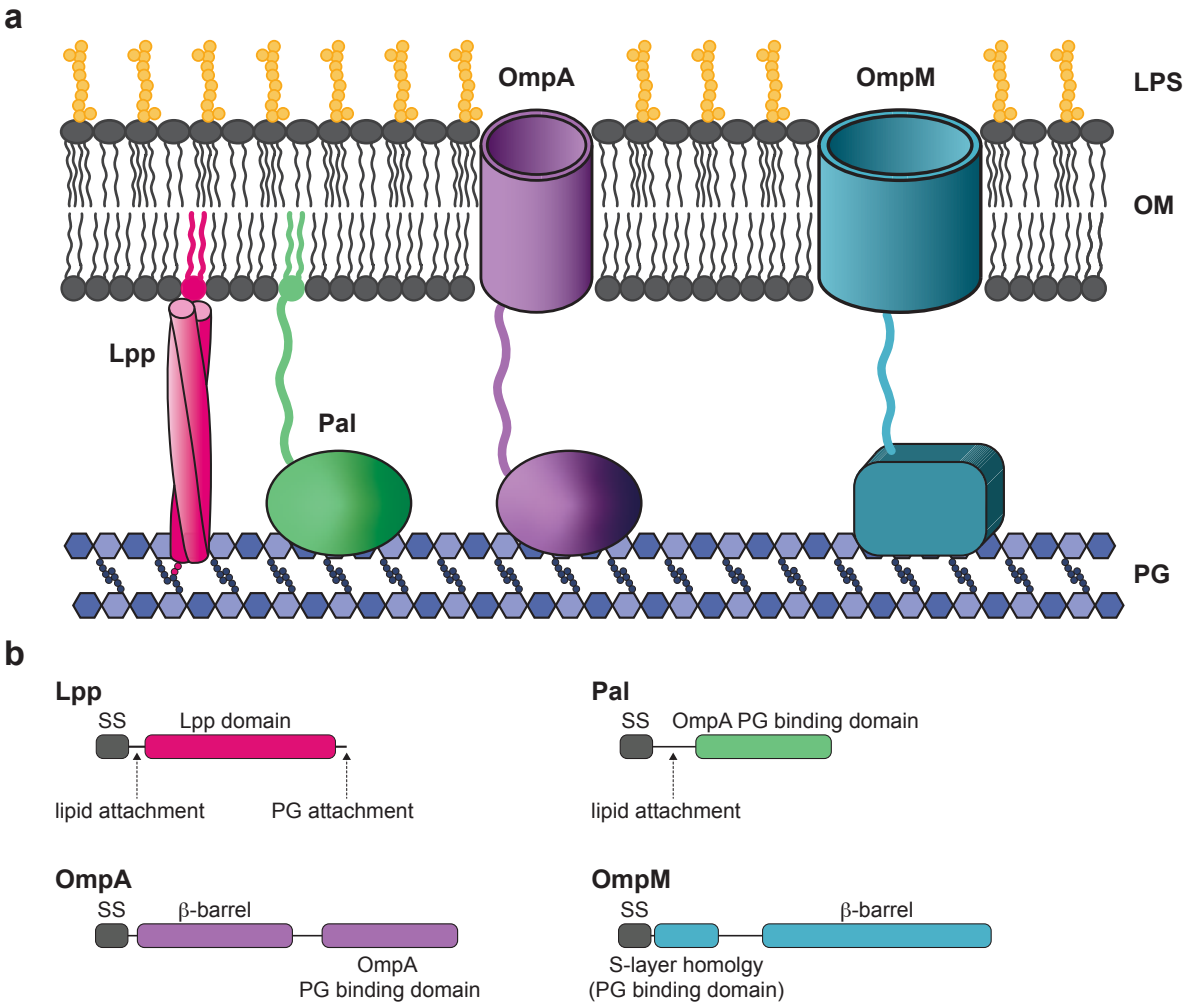

Figure 1. Schematic representation of the four major mechanisms for OM attachment to the cell wall: (**a**) Lpp, Pal and OmpA as the canonical *E. coli* systems, and OmpM as an alternative system reported from some Terrabacteria; (**b**) domain organization of the corresponding proteins. LPS means lipopolysaccharide, OM – outer membrane, PG – peptidoglycan, SS – signal sequence.

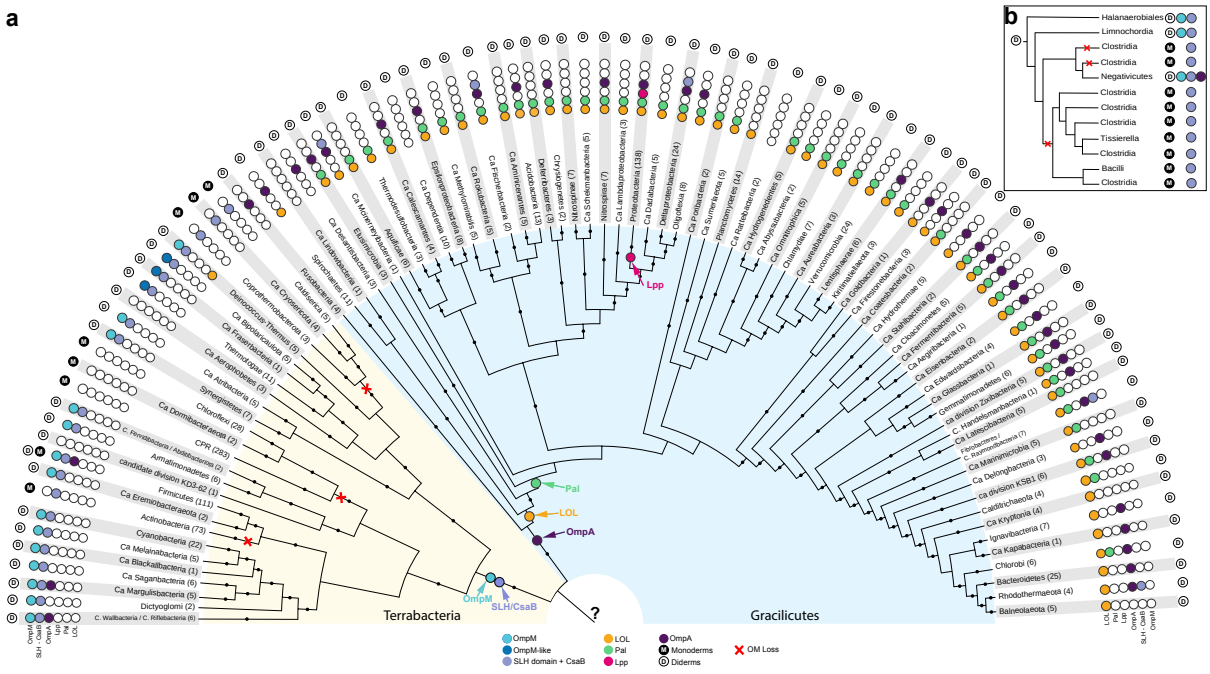

Figure 2. Distribution of major known OM attachment systems mapped on a reference phylogeny of Bacteria (a) and on a schematic tree of the Firmicutes (b). The phylogeny is based on the concatenation of RNA polymerase subunits β, β' and elongation factor IF-2 (2,206 amino-acid positions and 377 taxa) and is rooted in between the two large clades of the Terrabacteria and Gracilicutes, according to [4,72]. The tree was calculated using IQ-TREE version 1.6.3 with the model LG+C60+F+G and black dots indicate bootstrap values >90%. The presence of each of the four main attachment systems, of the Lol system, and of CsaB/SLH is marked with a colored dot. Arrows indicate the possible origin of each system. Red cross indicates the OM loss. The question mark in the LBCA indicates uncertainty on the presence of OmpM or OmpA (or yet another mechanism) (see Figure 6). Note that D indicates the presence of a classical OM (with or without LPS) as inferred either by experimental data or by the presence of Bam and other known OM systems. For this reason, Actinobacteria are marked as monoderms (M) even if some members have an OM made of mycolic acids, which is of more recent origin. In parentheses are indicated the number of genomes analyzed. All accession numbers are given in Supplementary Data Sheet 1A and 1B. The phylogenetic tree is available as a Newick file (Source Data for Figure 2.newick).

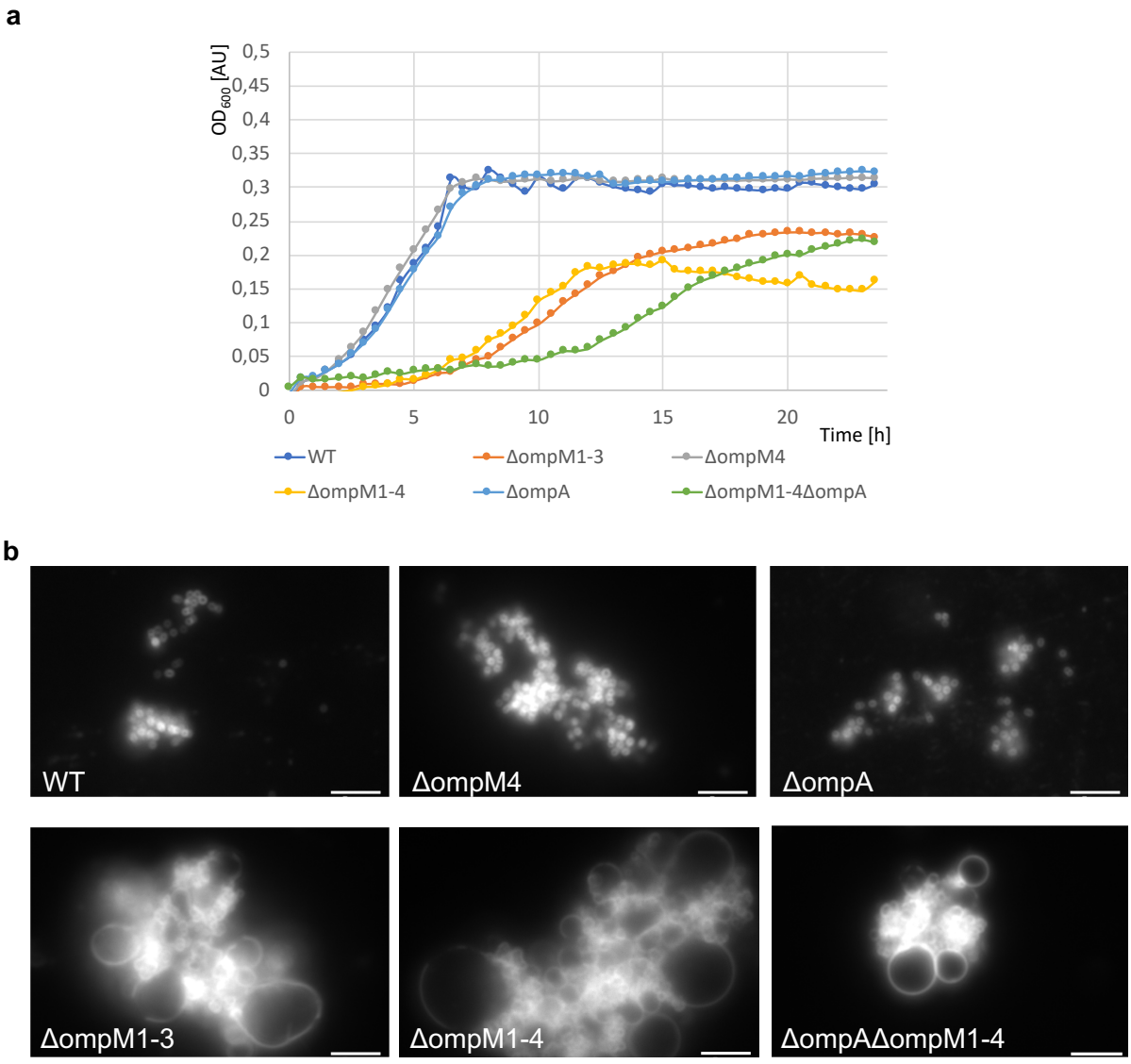

Figure 3. Phenotype of different *V. parvula* mutants generated in this study as compared to the WT. (a) – Growth curves. All data points represent the mean of a pentaplicate, error bars were omitted for sake of visibility. Cultures were made in BHILC medium in 96-well plates at 37°C under anaerobic conditions. **(b)** – Epifluorescence observation of cells labelled with the biological membrane staining dye FM 4-64 (Thermo Fisher Scientific). All scale bars represent 5 μm. The samples shown are representative of multiple (n>10) experiments.

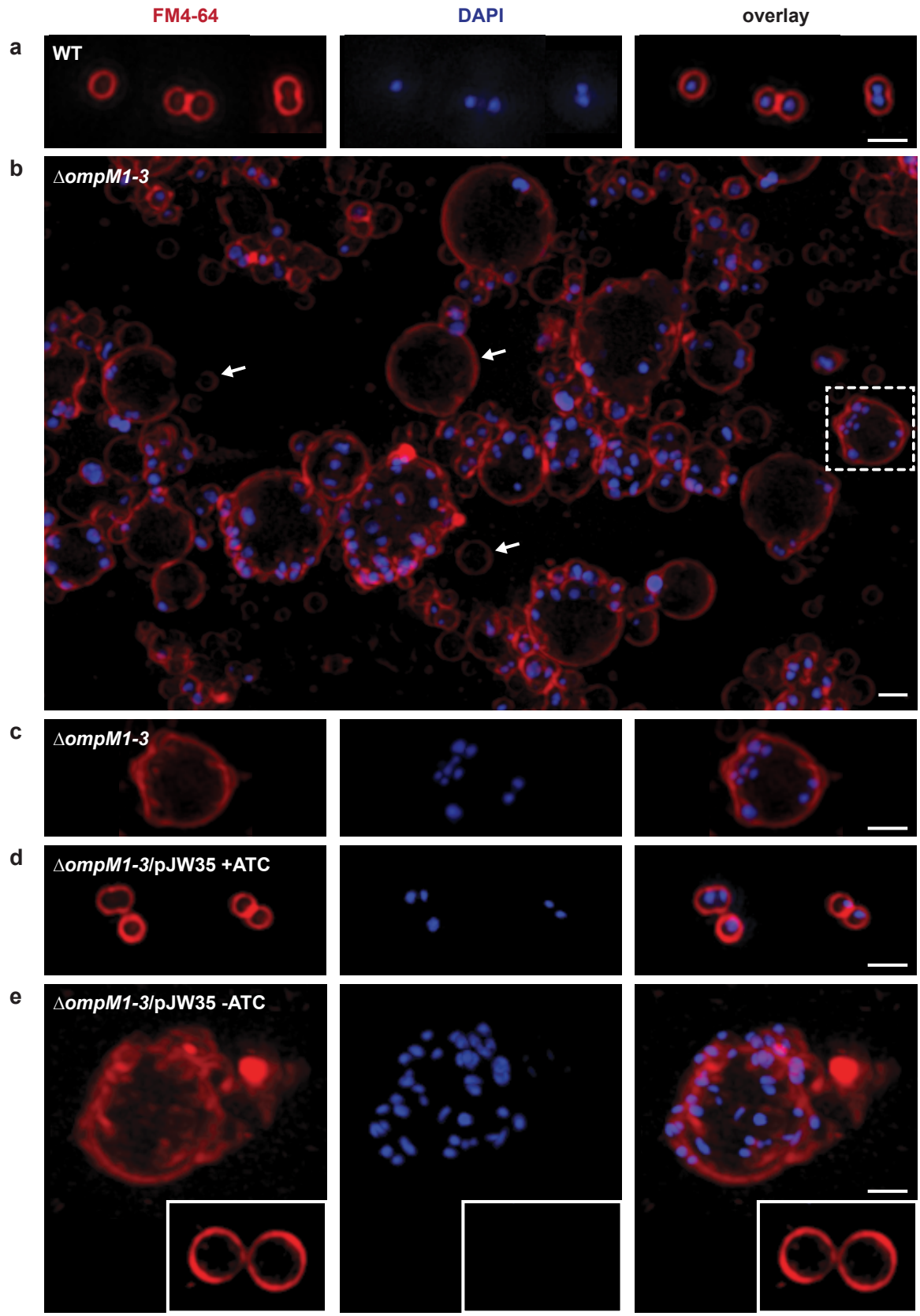

Figure 4. Membrane and DNA staining of representative *V. parvula* WT and Δ*ompM1-3* mutant cells imaged by 3D SIM. Cell membranes were stained with by

FM4-64 (red) and the DNA by DAPI (blue). (**a**) *V. parvula* WT. (**b** and **c**) Δ*ompM1-3* mutant of *V. parvula;* the panel (**b**) presents a large field of view where arrows indicate vesicles of different sizes devoid of any DNA signal. (**d**) Δ*ompM1-3* mutant of *V. parvula* complemented with pJW35 vector expressing OmpM1-HA under control of a *tet* promoter, induced overnight with 250 μg/l of anhydrotetracycline (+ATC). (**e**) Δ*ompM1-3* mutant of *V. parvula* complemented with an uninduced pJW35 vector (-ATC). Inlet shows membrane vesicles without DNA content. Scale bar in all images is 1 μm. The 3D-SIM acquisition was performed once, but the phenotype of the shown samples, as assessed by conventional fluorescence microscopy, is representative of multiple (n>20) experiments.

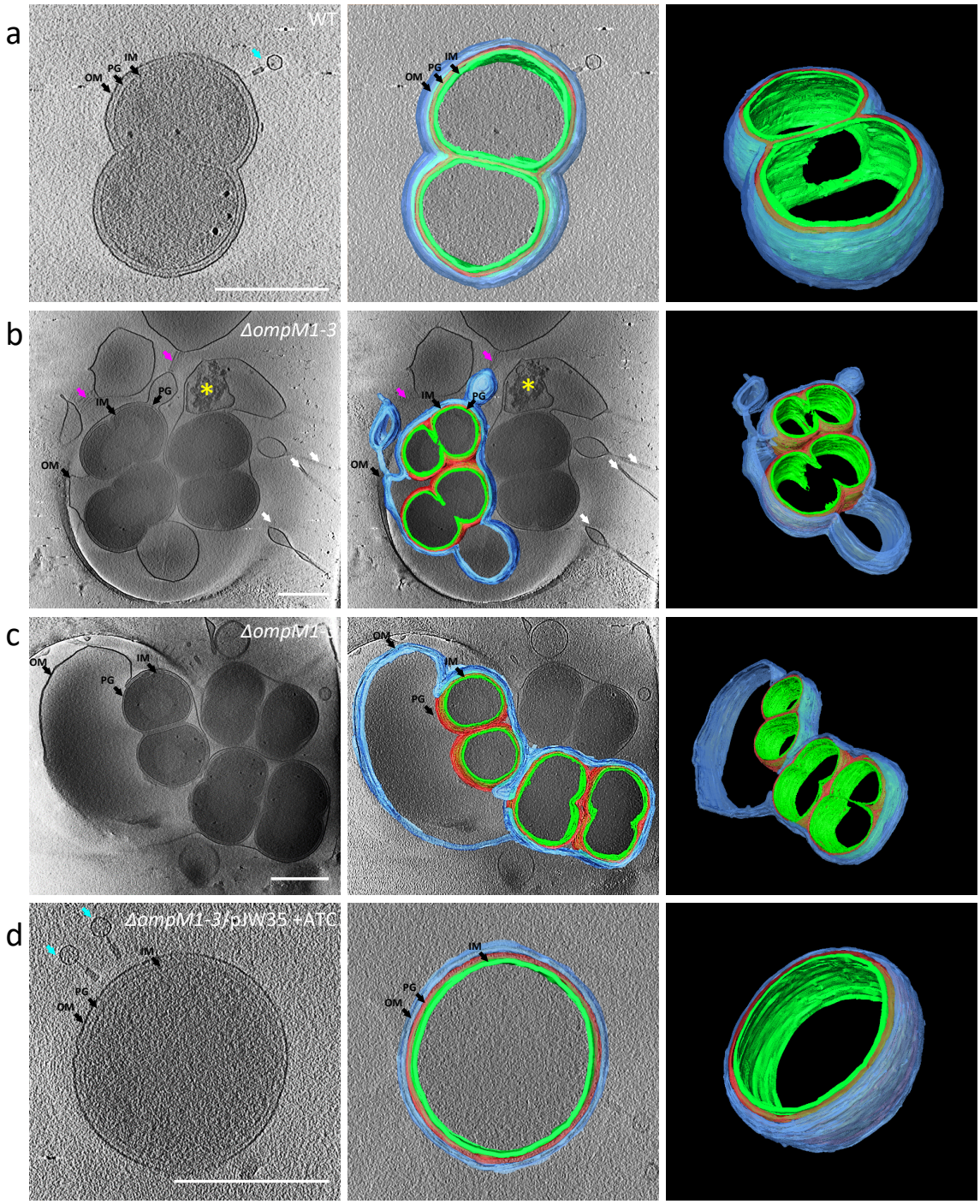
a
WT
IM
PG
OM
b
ΔompM1-3
IM
PG
OM
*
c
ΔompM1
OM
IM
PG
d
ΔompM1-3/pJW35+ATC
IM
PG
OM

Figure 5. Cryo-electron tomography of *V. parvula* WT and mutant cells. (a) – WT, **(b-c)** – Δ*ompM1-3* mutant; detached outer membrane forming blebs and vesicles is well visible, **(d)** - Δ*ompM1*-3 mutant of *V. parvula* complemented with pJW35 vector (expressing OmpM1-HA under control of *tet* promoter) induced overnight with 250 μg/l of anhydrotetracycline. Left panels represent a sum of 10 tomogram slices (16 nm), right panels a 3D rendering of the cell envelope structure based on manual segmentation of tomogram slices, middle panels are the superposition of a tomogram slice and the 3D rendering. OM / blue marking – outer membrane, PG / red marking – peptidoglycan, IM / green marking – inner membrane. White arrows show OM tubules. Pink arrows show a bundle of fimbriae-like structures connecting two OM. Yellow asterisk shows a degraded cell. Cyan arrows show bacteriophages (see Supplementary Results and Discussion 4). All scale bars represent 0.5 μm. Videos corresponding to panels a to d, containing all slices of the 3D tomogram reconstruction are available as Supplementary Movies S1 to S4. The CryoEM acquisition was performed twice, but the phenotype of the presented samples, as assessed by conventional fluorescence microscopy, is representative of multiple (n>20) experiments. The presence of phages, as visible in some Cryo-ET images, is not responsible for the observed phenotypes (see Supplementary Discussion).

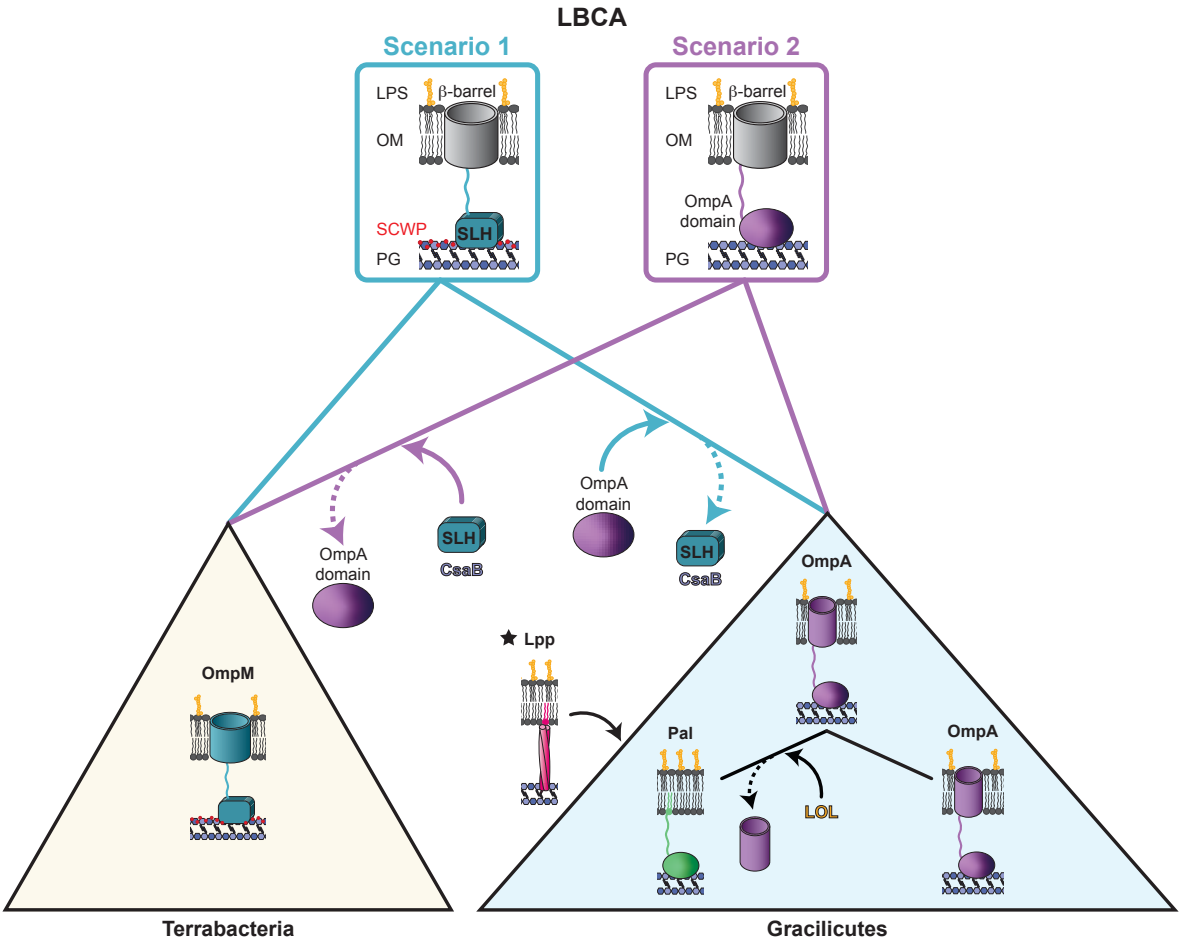

Figure 6. Two scenarios of evolution of OM tethering in Bacteria. Acquisitions are marked with full line arrows, and losses with dotted line arrows. In scenario 1, the LBCA tethered its OM via OmpM, and through interaction of the SLH domain with secondary cell wall polymers (SCWP) pyruvylated by the CsaB enzyme; this cell envelope configuration was inherited in diderm Terrabacteria, whereas in Gracilicutes the SLH domain was replaced by an OmpA domain leading to the OmpA tethering system, and the pyruvylated secondary cell wall polymers were lost along with CsaB. In scenario 2, the LBCA tethered its OM via OmpA; in Terrabacteria, the OmpA domain was replaced by the SLH domain upon appearance of the CsaB enzyme pyruvylating the SCWP, leading to the OmpM tethering system, whereas OmpA was conserved in Gracilicutes. In both scenarios, Pal arose from OmpA by replacement of

the porin domain with a lipid tail upon appearance of the Lol system to address lipoproteins to the OM. Finally, Lpp appeared *de novo* within *Gammaproteobacteria*.

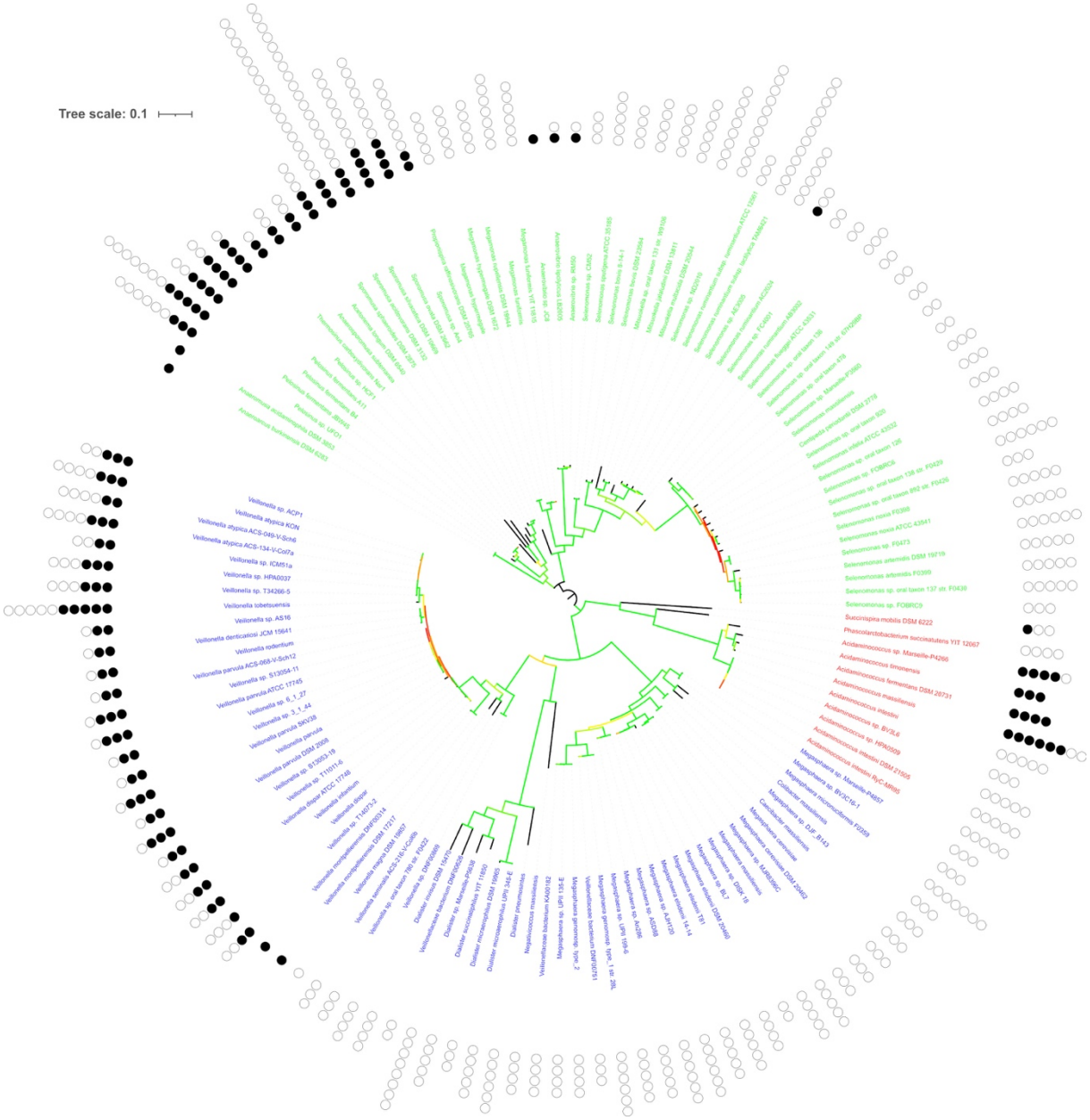

Extended Data Figure 1. Number of *ompM* copies per genome plotted on a reference Negativicutes tree containing 135 genomes. Selenomonadales are labelled in green, Acidaminococcales in red and Veillonellales in blue. The phylogeny is based on the concatenation of RNA polymerase subunits β, β′ and elongation factor IF-2 (3,027 amino-acid positions) The tree was calculated using IQTREE version 1.6.3 with the model LG+R5. Colours of branches represent bootstrap values from 80 (red) to 100 (green). The *ompM* copies present inside the OM gene cluster are marked by full circles,

those outside the cluster by empty ones. Source data is provided in the file “Source Data for Figure ED1.newick”.

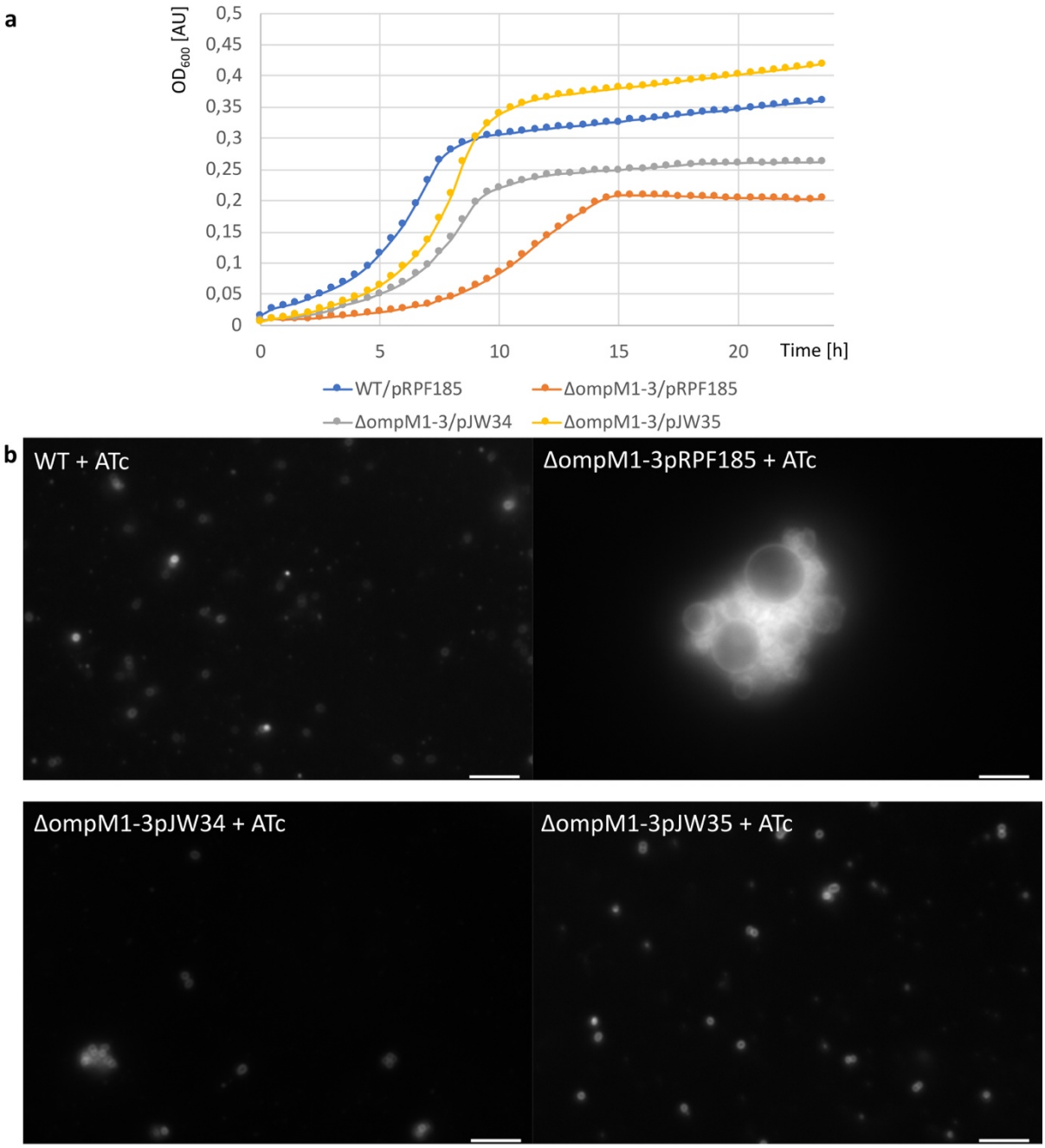

Extended Data Figure 2. Phenotypic complementation of the Δ*ompM1-3* mutant by production of native or HA-tagged OmpM1. (a) – Growth curves. All data points represent the mean of a pentaplicate, error bars were omitted for sake of visibility. Cultures were made in BHILC medium in presence of 250 μg/l of anhydrotetracycline in 96-well plates at 37°C under anaerobic conditions. pRPF185 – empty vector, pJW34 – a vector expressing native OmpM1 under the control of *tet* promoter, pJW35 – a vector expressing HA-tagged OmpM1 under the control of *tet* promoter. **(b)** –

Epifluorescence observation of cells labelled with the biological membrane staining dye FM 4-64 (Thermo Fisher Scientific). Overnight cultures were launched at 1/10th dilution of a stationary phase culture in SK medium at 37°C in anaerobic conditions in presence of aTc at 250 μg/l, before being labeled with the biological membrane staining dye FM 4-64 (Thermo Fisher Scientific) and observed by epifluorescence microscopy. Expression of either the native version of OmpM1 or its HA-tagged version led to complementation of the strong phenotype (formation of OM "bubbles" observed in the Δ*ompM1-3* mutant). Growth default of this mutant was also fully or partly complemented by native or HA-tagged OmpM1. All scale bars represent 5 μm. The samples presented are representative of multiple (n>20) experiments.

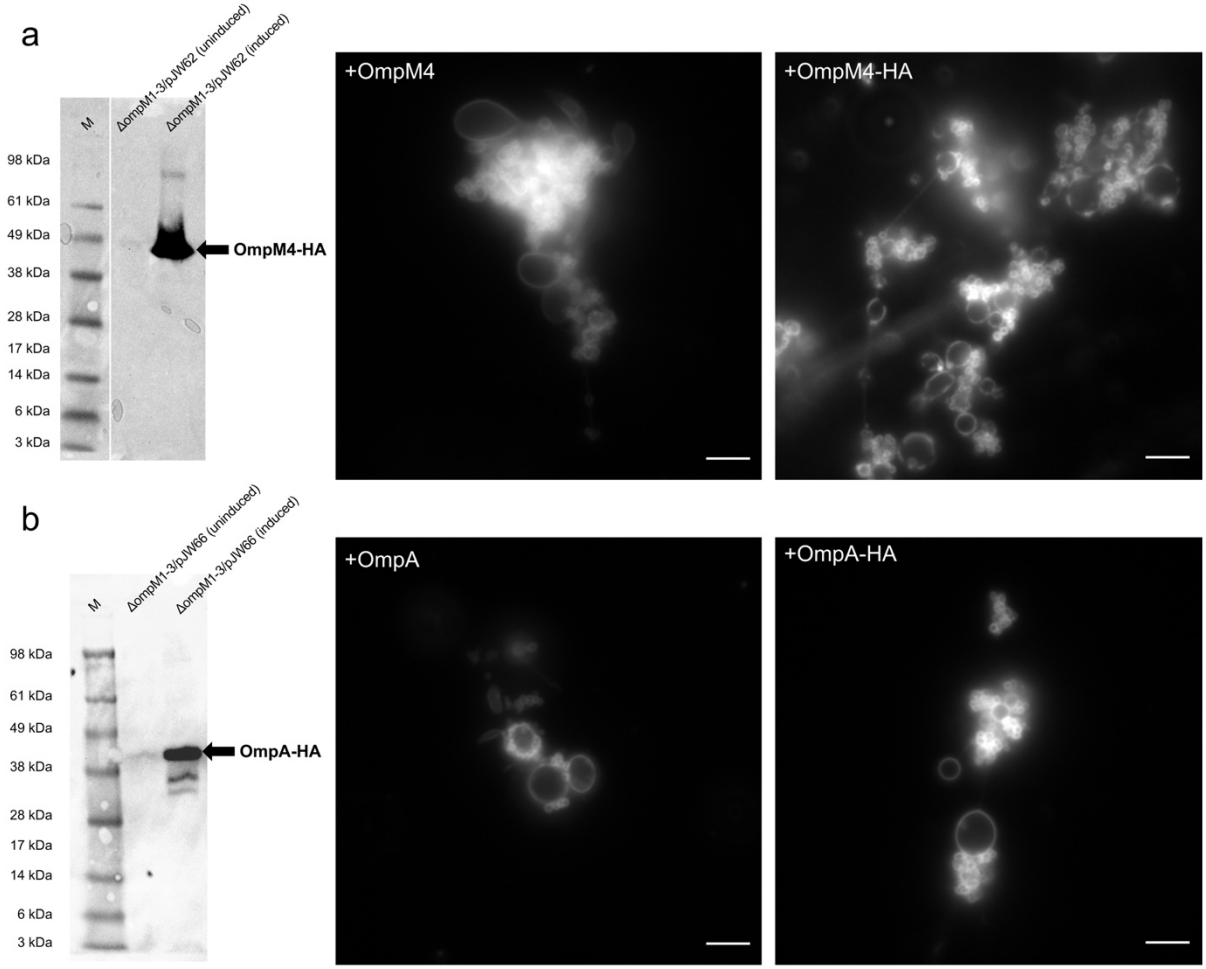

Extended Data Figure 3. The drastic phenotype of the Δ*ompM1-3* mutant cannot be complemented by expressing *in trans* OmpM4 or OmpA. In (**a**) the Δ*ompM1-3* was transformed with a plasmid expressing either native (pJW63) or HA-tagged (pJW62) OmpM4 from an aTc inducible promoter. In (**b**) the Δ*ompM1-3* was transformed with a plasmid expressing either native (pJW65) or HA-tagged (pJW66) OmpA from an aTc inducible promoter. Both OmpM4-HA and OmpA-HA were readily detected by western blot using an anti-HA primary antibody coupled to horse radish peroxydase when aTc was added at 250 μg/l (left panels). However, the strong phenotype of the Δ*ompM1-3* was not complemented by expressing either native or HA-tagged version of OmpM4, as well as native or HA-tagged version of OmpA, as shown on the right

panels following FM 4-64 epifluorescence. Scale bars represent 5 μm. The samples presented are representative of multiple (n>10) experiments.

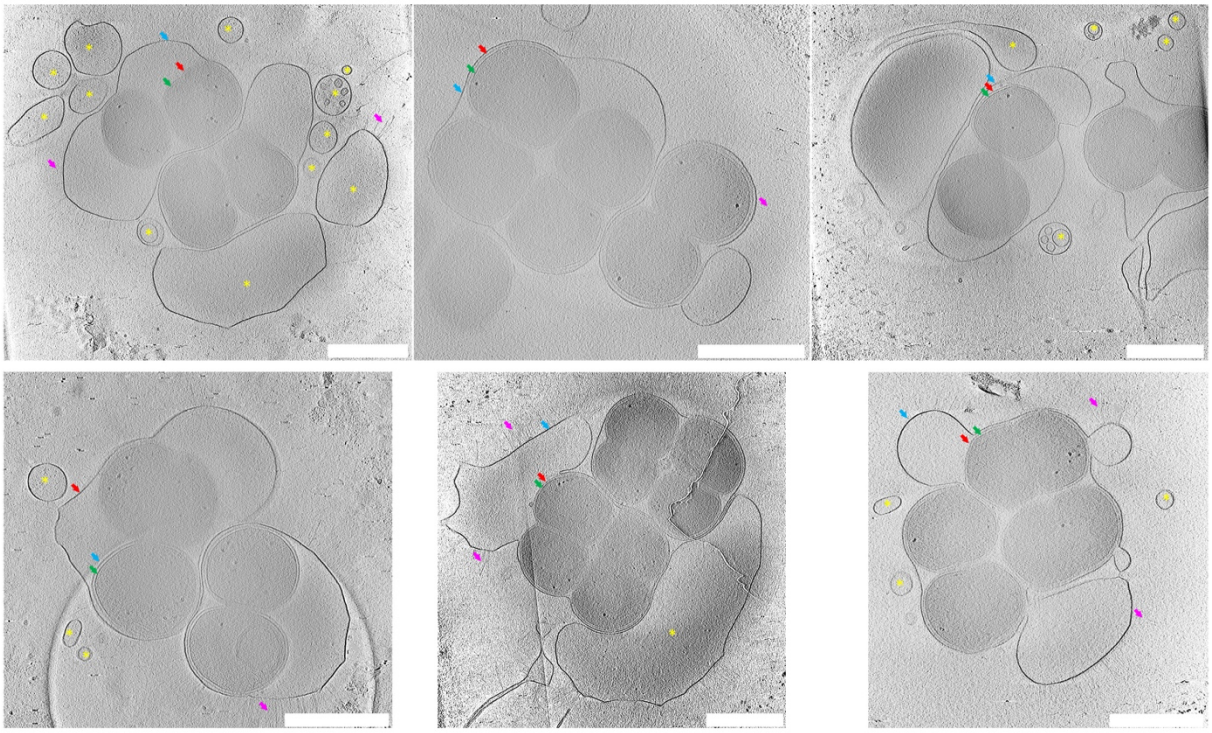

Extended Data Figure 4. Detailed characterization of the strong phenotype of the Δ*ompM1*-3 mutant using cryoelectron tomography. Cells of the Δ*ompM1-3* mutant were grown for 48h in SK medium before being prepared, deposited and observed using a 300kV Titan Krios (Thermo Fisher Scientific) transmission electron microscope. Different slices of cryoelectron tomography of different positions of a mesh grid containing the *ΔompM1-3* mutant are shown. Scale bars represent 0.5 μM, blue arrows OM, red arrows peptidoglycan, green arrows IM, grey arrows fimbriae, yellow asterisks indicate empty vesicles. The CryoEM acquisition was performed twice, but the phenotype of the presented samples, as assessed by conventional fluorescence microscopy, is representative of multiple (n>20) experiments.

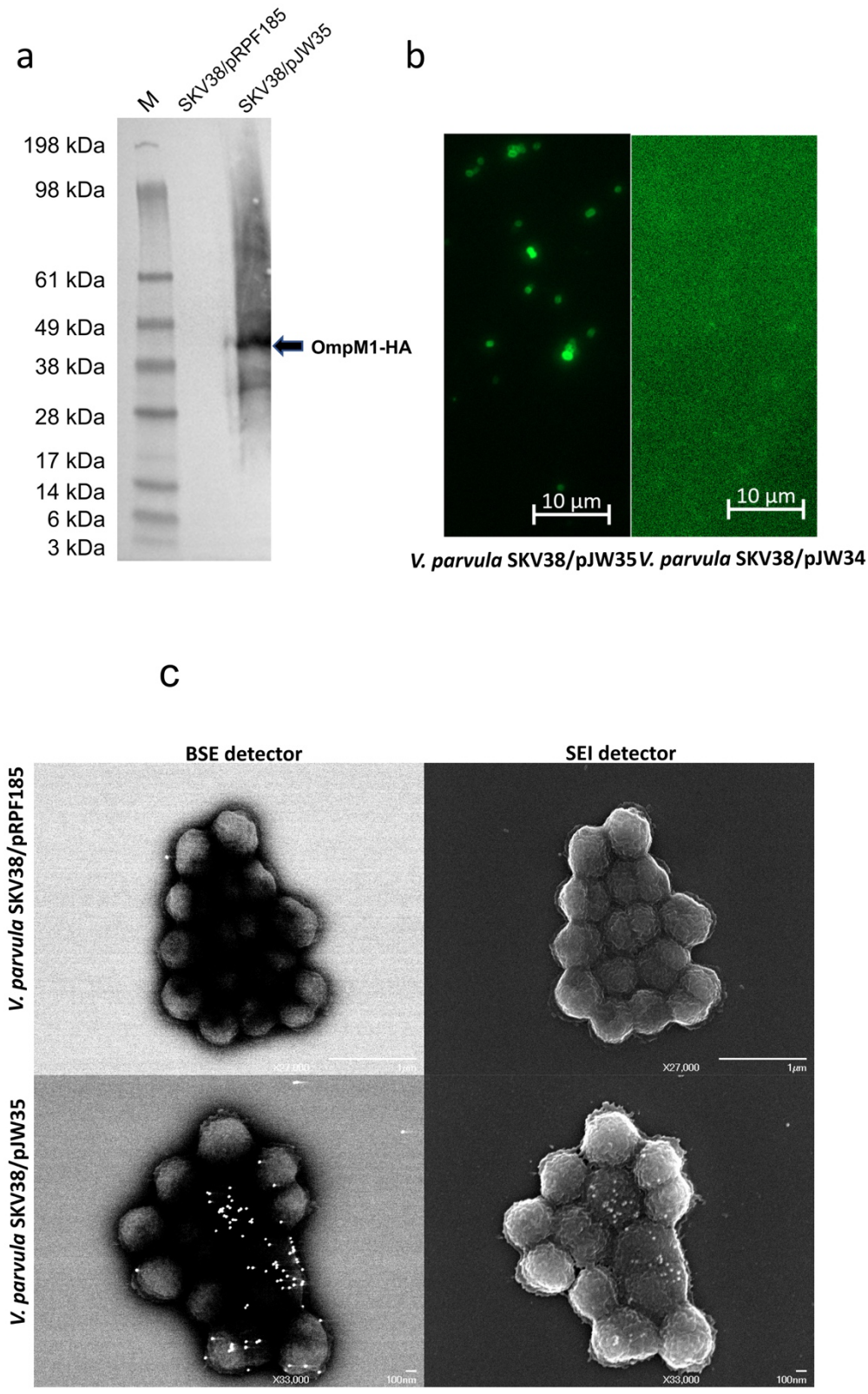

Extended Data Figure 5. OmpM1 is located in the outer membrane of *V. parvula*. Comparison of WT SKV38 strain of *V. parvula* containing pRPF185 (empty vector),

pJW34, a vector expressing untagged OmpM1, and pJW35, a vector expressing HA-tagged OmpM1 both under the control of *tet* promoter. All cultures were induced overnight with 250 μg/l anhydrotetracycline. In (**a**), we used an anti HA primary and antibodies coupled to horse radish peroxidase (HRP) to detect the expression of OmpM1-HA (arrow) from pJW35 by Western blot. M corresponds to SeeBlue Plus Prestained Protein Standard (Invitrogen). In (**b**), we performed immunofluorescence microscopy of WT cells expressing either OmpM1-HA (pJW35) or native OmpM1 (pJW34) using an anti-HA antibody coupled to fluorescein. Cells were non-permeabilized. While native OmpM1 was not detectable, OmpM1-HA that contains the HA tag in one of the predicted outer loops of its beta-barrel could be detected as all around the cell, confirming that it located in the outer membrane and is surface exposed. Surface exposition of tagged OmpM1 expressed from pJW35 was confirmed using Scanning Electron Microscopy in (**c**). We used anti-HA primary antibodies and secondary antibodies coupled to 20 nm gold particles on non-permeabilized cells. Images were obtained using a JEOL JSM 6700F field emission scanning electron microscope and with a backscattered electrons detector (BSE) to detect the gold labelling and with a secondary electron detector (SEI) to image the surface of the sample. The acquisitions were performed once.

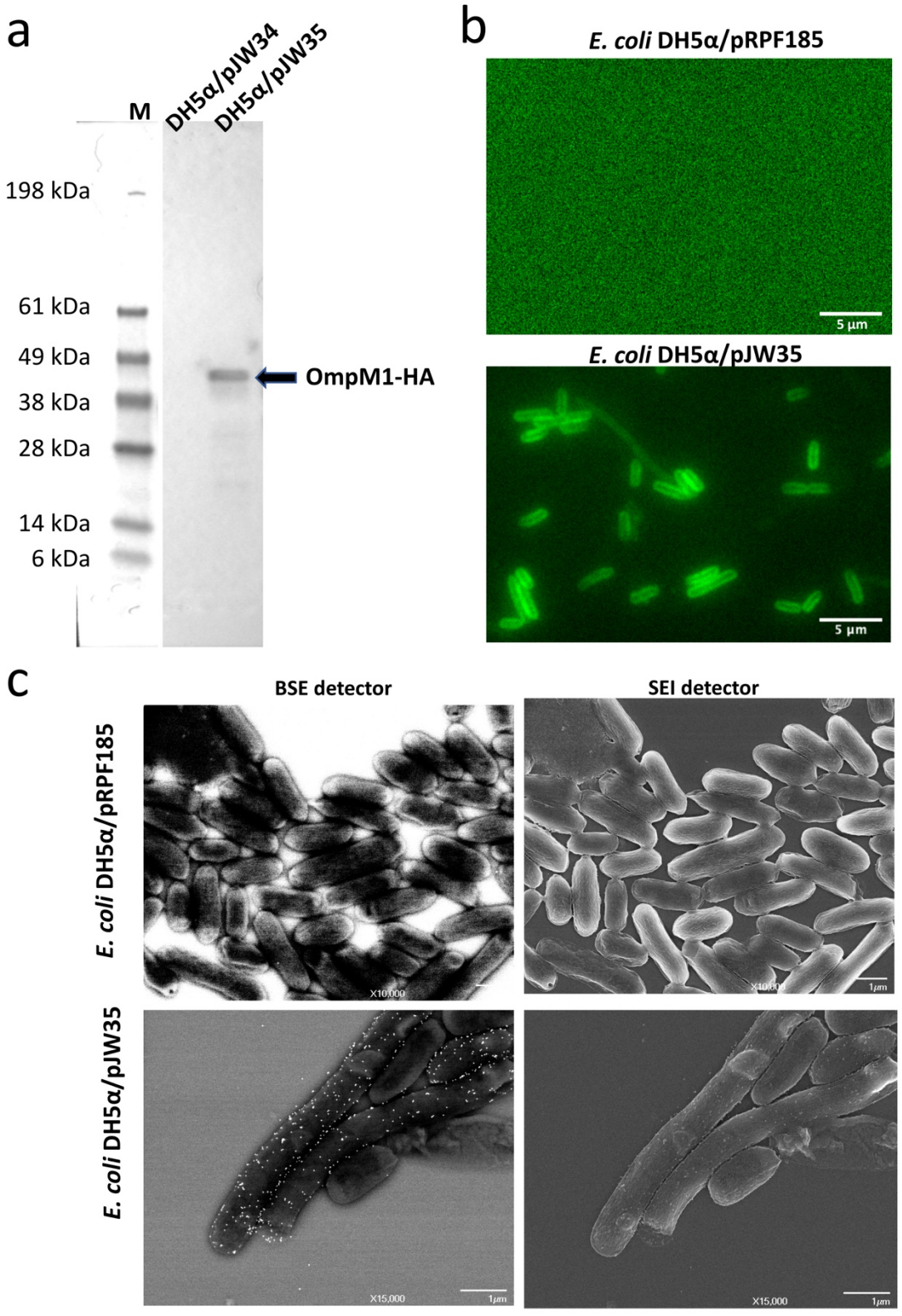

Extended Data Figure 6. OmpM1 is detected at the cell surface when expressed in *E. coli*. As for supplementary Figure S10 we compared *E. coli* cells expressing containing pRPF185 (empty vector), pJW34, a vector expressing untagged OmpM1, and pJW35, a

vector expressing HA-tagged OmpM1 both under the control of *tet* promoter. All cultures were induced overnight with 250 μg/l anhydrotetracycline. In (**a**), we used an anti-HA antibodies coupled to HRP to detect, in *E. coli*, the expression of OmpM1-HA (arrow) from pJW35 by Western blot, while the non-tagged native OmpM1 expressed from pJW34 could not be detected. M corresponds to SeeBlue Plus Prestained Protein Standard (Invitrogen). In (**b**), we performed immunofluorescence microscopy of *E. coli* cells expressing no OmpM1 (empty vector pRPF185) or OmpM1-HA (pJW35) using an anti-HA antibody couple to fluorescein. *E. coli* cells were non-permeabilized. OmpM1-HA that contains the HA tag in one of the predicted outer loops of its beta-barrel could be detected as all around *E. coli* cells, confirming that it located in the outer membrane and is surface exposed also in this bacterium, therefore suggesting that it could be transported and inserted in the outer membrane of a classical diderm bacterium. Surface exposition of tagged OmpM1 expressed from pJW35 in *E. coli* was confirmed using Scanning Electron Microscopy in (**c**). We used anti-HA primary antibodies and secondary antibodies coupled to 20 nm gold particles on non-permeabilized cells. Images were obtained using a JEOL JSM 6700F field emission scanning electron microscope and with a backscattered electrons detector (BSE) to detect the gold labelling and with a secondary electron detector (SEI) to image the surface of the sample. The acquisitions were performed once.

Substance	WT	*ΔompM1-3*	*ΔompM4*	*ΔompA*	*ΔompM1-4*	*ΔompA ΔompM1-4*	WT pRPF185 + ATc	*ΔompM1-3* pRPTF185 + ATc	*ΔompM1-3* pJW34 + ATc	*ΔompM1-3* pJW35 + ATc
Sodium deoxycholate	300 mg/l	5 mg/l	300 mg/l	300 mg/l	5 mg/l	<0.6 mg/l	300 mg/l	9 mg/l	150 mg/l	300 mg/l
EDTA	2500 μM	156 μM	2500 μM	2500 μM	156 μM	<5 μM	2500 μM	313 μM	1250 μM	2500 μM
SDS	100 mg/l	3 mg/l	100 mg/l	100 mg/l	3 mg/l	<0.2 mg/l	50 mg/l	3 mg/l	25 mg/l	50 mg/l
Vancomycin	>1000 mg/l	31 mg/l	>1000 mg/l	> 1000 mg/l	31 mg/l	<1 mg/l	500 mg/l	16 mg/l	63 mg/l	250 mg/l

Extended Data Table 1. Minimum inhibitory concentrations (MIC) of outer membrane stress inducing molecules on the five mutant strains with respect to the WT. The last four columns correspond to the complementation assay of the *ΔompM1-3* mutant. pRPF185 – empty vector. pJW34 – vector expressing native OmpM1 under the control of *tet* promoter. pJW35 – vector expressing a HA-tagged version of OmpM1 under the control of *tet* promoter. +ATc – culture realized in presence of 250 μg/l of anhydrotetracycline under chloramphenicol (25 mg/l) selection. The data presented in the table are a result of a duplicate.